iScience

Article

Trop-1/EpCAM Thr115 is a driver of hyperproliferative cell repair and of severe lung damage in COVID-19

Graphical abstract

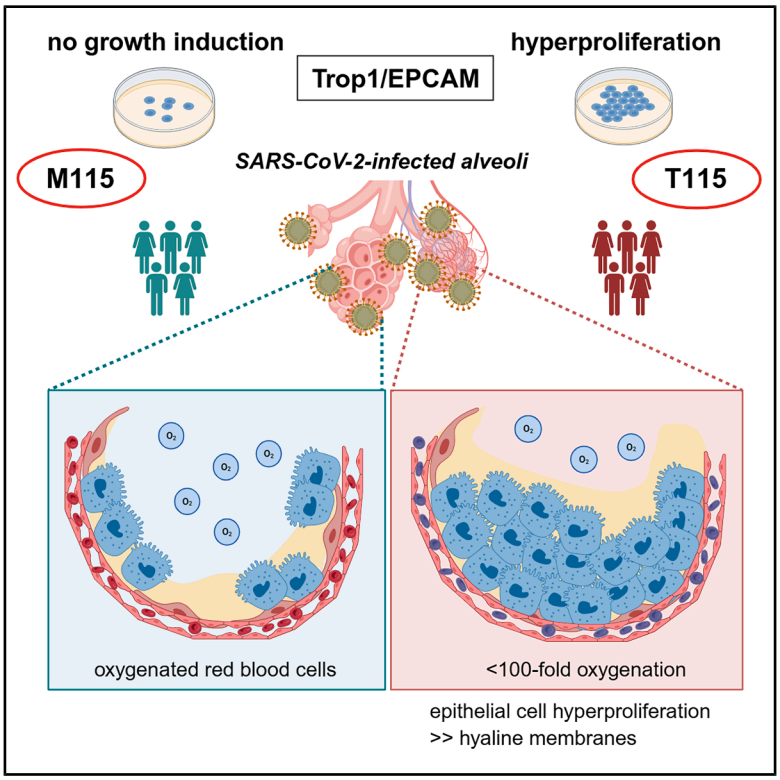

Highlights

- The Trop-1/EpCAM Thr115 polymorphism associates with severe COVID-19 outcome
- Trop-1/EpCAM Thr115 drives proliferation of normal and transformed cells
- Trop-1/EpCAM Thr115 drives hyperproliferative wound repair in the lungs in COVID-19
- Trop-1/EpCAM Thr115 lung repair leads to a >100-fold reduction in oxygen diffusion

Authors

Margherita Baldassarri, Marco Trerotola, Giulia Brunelli, ..., Alessandra Renieri, Chiara Fallerini, Saverio Alberti

Correspondence

alessandra.renieri@unisi.it (A.R.), salberti@unime.it (S.A.)

In brief

Microbiology; Virology; Cell biology

Baldassarri et al., 2026, iScience *29*, 117361
September 18, 2026
https://doi.org/10.1016/j.isci.2026.117361

CellPress

iScience

CellPress
OPEN ACCESS

Article

Trop-1/EpCAM Thr115 is a driver of hyperproliferative cell repair and of severe lung damage in COVID-19

Margherita Baldassarri,[1,2,11] Marco Trerotola,[3,4,11] Giulia Brunelli,[1,2] Noemi La Francesca,[5] Laura Bergantini,[6] Benedetta Tella,[1,2] Giulia Rollo,[1,2] Cecilia Altemura,[1,2] Vera Giacomazzi,[1,2] Emanuela Guerra,[3,4] Martina Ceci,[3,4] Ludovica Pantalone,[3,4] Samantha Minetto,[1,2] Elena Bargagli,[6] Cristoforo Pomara,[7] Rossano Lattanzio,[3,8] Antonino Moschella,[9] Federica Maria Previtera,[9] Cristiana Bellan,[5] Network for Italian Genomes[13], GEN-COVID Multicenter Study[13] Alessandra Renieri,[1,2,10,*] Chiara Fallerini,[1,2,12] and Saverio Alberti[9,12,14,*]

[1]Medical Genetics, University of Siena, 53100 Siena, Italy
[2]Med Biotech Hub and Competence Center, Department of Medical Biotechnologies, University of Siena, 53100 Siena, Italy
[3]Center for Advanced Studies and Technologies (CAST), University "G. d'Annunzio" of Chieti-Pescara, 66100 Chieti, Italy
[4]Department of Medical, Oral and Biotechnological Sciences, University "G. d'Annunzio" of Chieti-Pescara, 66100 Chieti, Italy
[5]Section of Pathology, Department of Medical Biotechnologies, University of Siena, 53100 Siena, Italy
[6]Respiratory Disease Unit, Department of Medical Sciences, University Hospital of Siena (Azienda Ospedaliera Universitaria Senese, AOUS), 53100 Siena, Italy
[7]Division of Legal Medicine, University of Catania, 95100 Catania, Italy
[8]Department of Innovative Technologies in Medicine & Dentistry, G. d'Annunzio University, 66100 Chieti, Italy
[9]Unit of Medical Genetics, Department of Biomedical Sciences-BIOMORF, University of Messina, 98125 Messina, Italy
[10]Genetica Medica, Azienda Ospedaliero-Universitaria Senese, 53100 Siena, Italy
[11]These authors contributed equally
[12]These authors contributed equally
[13]Further details can be found in the supplemental information
[14]Lead contact
*Correspondence: alessandra.renieri@unisi.it (A.R.), salberti@unime.it (S.A.)
https://doi.org/10.1016/j.isci.2026.117361

SUMMARY

SARS-CoV-2 lung infection triggers an acute reaction that can severely impair oxygen exchange. However, the underlying molecular processes are poorly understood. The *TROP1/EPCAM* p.M115T polymorphism was found associated with COVID-19 severity. We discovered here that the T115 Trop-1/EpCAM is a driver of cell growth, whereas M115 Trop-1/EpCAM has little, if any, cell growth induction capacity. *TROP1/EPCAM* knockout mice showed altered proliferation of embryonic stem cells. The Trop-1/EpCAM T115 allele was then found to drive hyperproliferative capacity in murine fibrosarcoma cells. Corresponding growth stimulation was shown in human colon cancer cells, through CRISPR-Cas9 ablation of the endogenous *TROP1/EPCAM* and comparative transfection of *TROP1/EPCAM* p.T115 (T-mod) or p.M115 (M-mod) alleles. In COVID-19 patients, T115 Trop-1/EpCAM was shown to cause aberrant, hyperproliferative wound repair in SARS-CoV-2-damaged lung alveoli that led to critical oxygen-exchange impairment. Analysis of COVID-19 patient lungs at autopsy showed hyperproliferation of T115 Trop-1/EpCAM$^+$ epithelial cells over the alveolar epithelium damaged by the infection. This correlated with T115 Trop-1/EpCAM$^+$ inflammatory cells hyperproliferation and alveolar hyaline membrane formation. These multi-layered barriers were computed to reduce oxygen diffusion by up to 100-fold. Our findings indicate an unanticipated mechanism for lung damage by T115 Trop-1/EpCAM, and suggest a potential target for corresponding therapeutic approaches.

INTRODUCTION

Years after the beginning of the COVID-19 pandemic, one of the major challenges remains the identification of the molecular mechanisms that determine the severity the disease. Age, sex, and pre-existing pathological conditions were shown to affect clinical outcomes.[1–3] Genetic factors can play a key, though incompletely understood, role in disease progression.[4–18] The application of a machine learning model to exome sequencing data of the GEN-COVID consortium (n = 2,446) allowed us to identify the p.Met115Thr (M115T) (rs1126497; c.344T>C) polymorphism of the *TROP1/EPCAM* gene as an independent prognostic factor for the course of COVID-19. Additional genetic variants have been associated with COVID-19 severity, among them polymorphisms at a chromosome 3p21.31 locus (which encompasses genes such as the LZTFL1 transcription factor,

Table 1. Allele frequency of the rs1126497 (c.344T>C) polymorphism in the *TROP1/EPCAM* gene in the European (non-Finnish) population (gnomAD), and in the GEN-COVID cohort (cases plus controls)

Nucleotide	Amino acid	Allele frequency gnomAD	Allele frequency GEN-COVID cohort	Population
c.344T	Met115	0.57	0.63	European (non-Finnish)
c.344C	Thr115	0.43	0.37	European (non-Finnish)

the SLC6A20 Solute Carrier Family 6 Member 20, the CCR9 chemokine and the CXCR6 chemokine receptor).[4] Association of a polymorphism of *TROP1/EPCAM*, a gene that takes part to maintaining the architecture of epithelial tissues,[19–22] to COVID-19 severity suggested an involvement of the T115 allele in lung epithelial cell pathology.[23,24]

The *TROP1/EPCAM* gene[25] (STAR Methods – nomenclature) encodes Trop-1/EpCAM,[19,20] a monomeric transmembrane glycoprotein that transduces an intracellular calcium signal.[21] In epithelial cells, Trop-1/EpCAM takes part in the formation of cell-cell adhesion structures at contact sites of adjacent cells.[22] Trop-1/EpCAM does not belong to other known cell-cell adhesion molecule classes[26] and, despite early indications,[27] rather than being an adhesion molecule itself,[28,29] it downregulates the adhesive function of E-cadherin and β-catenin.[30]

Trop-1/EpCAM is expressed by proliferating epithelial cells,[19,31] and by progenitor cells of epithelial,[32–35] germinal,[36] and hematopoietic[37] lineages. Of relevance, Trop-1/EpCAM is also expressed by a vast fraction of human cancers,[32,38,39] whereby the Trop-1/EpCAM$^+$ CD44$^+$ cells comprise the proliferating compartment/progenitor cells.[40] Activation of Trop-1/EpCAM by proteolytic cleavage[41,42] triggers tumor cell growth[19,43] and malignant progression.[44–46]

Here, we show that a frequent polymorphism (p.M115T) of the *TROP1/EPCAM* gene[47] is a host factor that drives lung damage in severe COVID-19 disease. Trop-1/EpCAM is a cancer driver and large-scale tumor DNA sequencing projects (www.cbioportal.org/datasets) have frequently listed the *TROP1/EPCAM* p.M115T (rs1126497; c.344T>C) polymorphism as a mutation (https://www.uniprot.org/uniprotkb/P16422/entry), largely because of lack of comparison of tumor sequences with germline data.

In this article, we discovered that the T115 Trop-1/EpCAM is a driver of tumor cell growth, whereas M115 Trop-1/EpCAM has little, if any, cell growth induction capacity. We assessed M115 versus T115 Trop-1/EpCAM alleles for induction of differential growth in experimental cell models. We obtained *mTrop1* inactivation by targeted gene replacement[48] in the TBV-2 mouse embryonic stem (ES) cells.[49] We found a lower proliferative capacity of hemizygous *TROP1/EPCAM* ES cells, which indicated a quantitative response to endogenous *TROP1/EPCAM* genes. Transfection of fibrosarcoma L cells for T115 versus M115 Trop-1/EpCAM alleles showed that the T115 allele confers hyperproliferative properties, whereas the M115 allele shows essentially no capacity to induce cell proliferation. Intermediate proliferation rates were shown in T115/M115 heterozygous cells, suggesting a quantitative relationship versus T115 Trop-1/EpCAM expression levels. Formal confirmation of these findings was obtained by transgenesis of the two alleles in *TROP1/EPCAM* CRISPR-Cas9-ablated KM12SM human colon cancer cells.[50] In this cellular system, growth-driving capacity was only retained by the T115 allele.

These findings led us to speculate that T115 Trop-1/EpCAM plays a pivotal role as an inducer of proliferation of wound-healing cells in the damaged lung epithelium in COVID-19 patients. Immunohistochemistry (IHC) analysis of the lungs of COVID-19 patients at autopsy demonstrated induction of Trop-1/EpCAM expression in alveolar type 2 (AT2) pneumocytes from the earliest stages of epithelial damage repair. This was followed by overproliferation of T115 Trop-1/EpCAM$^+$ cells, and by the formation of multi-stratified layers of alveolar cells, which severely impeded oxygen diffusion. T115 Trop-1/EpCAM expression was also shown in inflammatory cells, where it correlated with immune cell proliferation in lung tissues of COVID-19 patients with severe disease.[51] This hyperinflammatory state led to intraalveolar hyaline membrane formation, which further reduced oxygen permeability.

These findings indicate an unanticipated path toward acute lung damage after viral infection that associates to severe COVID-19 outcomes.

RESULTS

p.M115T *TROP1/EPCAM* gene associates with COVID-19 severity

By applying post-Mendelian genetic models to a cohort of 2,446 SARS-CoV-2 infected subjects with different disease severity, we identified the *TROP1/EPCAM* (NM_002354.3) p.M115T (rs1126497, c.344T>C) polymorphism as contributing to disease outcome.[23,24]

In order to assess the pathological role of this polymorphism, patients showing severe COVID-19 (cases) and infected individuals with no signs of disease (controls) were compared (n = 1848). The identified frequencies were in Hardy-Weinberg equilibrium. The minor allele frequency in our cohort was similar (37.05%) to that reported in the Network for Italian Genomes database (NIG; http://nigdb.cineca.it/) (37.3%). The polymorphic allele frequency in our cohort was correspondingly similar to that reported for the European (non-Finnish) population (gnomAD) (Table 1). We subdivided patients into two categories, those having the *TROP1/EPCAM* p.T115 polymorphism in heterozygous or homozygous state and those homozygous for the p.M115 allele (Table 2). We found that homozygotes for p.T115 have an increased risk for severe COVID-19 (odds ratio [OR] of 1.52 confidence interval [CI] 95% 1.15–2.01), with a p value of 2.9×10^{-3} (Table 3).

TROP1/EPCAM sequence variants in cancer genomes

Trop-1/EpCAM expression impacts on tumor progression of breast tumors,[38,52–55] non-small cell lung cancer,[47,56,57] colon cancer,[58] and others. In cancer cells, Trop-1/EpCAM functions as a proliferation driver, upon overexpression as a wild-type molecule.[19]

Table 2. Number of patients with the rs1126497 (c.344T>C) polymorphism in the *TROP1/EPCAM* gene in the GEN-COVID cohort (cases plus controls)

	Trop-1/EpCAM amino acids at position 115			
	M115/M115 homo	M115/T115 hetero	T115/T115 homo	Total
Number of patients	713	887	248	1,848

Table 3. Statistical analysis for Trop-1/EpCAM polymorphism association with disease risk in the GEN-COVID cohort

Phenotype	M115T_homo T	Other	Total
Severe	160	871	1031
Nonsevere	88	729	817
Total	248	1,600	1,848

OR = 1.52 (95% CI 1.15–2.01) $p = 2.9 \times 10^{-3}$.

Systematic analysis for M115T variant prevalence and function was conducted c/o the web repositories at the Broad institute, International Cancer Genome Consortium (ICGC), Global Variome Shared Leiden Open Variation Database (LOVD), cBioportal, and ClinVar. The M115T polymorphism was broadly misclassified as a mutation in cancer sequence databanks (Figures 1A and 1B). The association to Lynch syndrome[61] and to pediatric cancers was originally taken to support a mutagenetic model. These findings may now be reinterpreted as supporting a tumor progression role of a germline T115 Trop-1/EpCAM variant.

Structure of M115 versus T115 Trop-1/EpCAM

Very little experimental evidence was available on the impact of the M115T polymorphism on Trop-1/EpCAM structure and function.[55,61,62] Comparison of Trop-1/EpCAM T115 versus M115 transfectants did not reveal sizable differences in expression levels, suggesting a limited, if any, impact of this polymorphism on the transport and stability of the two polymorphic Trop-1/EpCAM. Sorting Intolerant From Tolerant (SIFT) analysis (https://sift.bii.a-star.edu.sg/) can predict whether an amino acid substitution affects protein function,[63] based on sequence homology and on the amino acids physical properties. SIFT computations indicated that Thr and Met possess high scores as tolerated residues at the 115 position (Figure S1).

The T115 Trop-1/EpCAM (4mzv) structure was used as a template to obtain the structure of the M115 Trop-1/EpCAM[59,60] (Figures 1C–1E). The T115 and M115 Trop-1/EpCAM variants were subsequently superimposed with PyMol (https://www.pymol.org/) (Figure 1C). This showed no apparent divergence between the two structures. Formal assessment was conducted via the Ramachandran plot analysis (Figure 1F). This revealed essential invariance of the Φ and Ψ peptide bonds throughout the structures of T115 and M115 Trop-1/EpCAM, suggesting limited differential impact of the T115 versus M115 polymorphic residues on the Trop-1/EpCAM structure.

T115/M115 was shown to be solvent-exposed residue in a surface cavity of the molecule, which is essentially filled by the hydrophobic side chain of Met (Figures 1D and 1E). This and the polar nature of the side chain of Thr suggested that potential interactions of binding partner(s) to this region of Trop-1/EpCAM may be altered by a polymorphic change to Met.

mTrop1 +/– knockout cells show a reduced proliferative capacity

We had previously shown that Trop-1/EpCAM can play a key role in the control of cell proliferation.[19] Hence, we investigated the role of Trop-1/EpCAM T115 versus M115 alleles in driving cell growth.

Inactivation of the mouse *mTrop1* was obtained by targeted gene replacement[48] in the TBV-2 murine ES cell line.[49] A 1,267 bp DNA fragment located 85 bp upstream of exon 1 (5′ homology region [HR]) was PCR-amplified from TBV-2 ES genomic DNA and a 3,700 bp DNA fragment from intron 3 to intron 5 (3′ HR) was PCR-amplified from a C57/Bl6 mouse bacterial artificial chromosome (BAC) library. The targeting vector containing the 5′ and 3′ HRs flanking the floxed phosphoglycerate kinase (PGK)-*neo* cassette was linearized and electroporated into the TBV-2 ES cells. Homologous recombination at the *mTrop1* locus was predicted to create a null allele by replacing a 2,341-bp region, containing the transcriptional and translational start sites and the first 27 codons of the *mTrop1* open reading frame (ORF), with the PGK-*neo* selection cassette (Figure 2A). Candidate gene-replacement ES clones were selected by resistance to G418/ganciclovir.

Growth of *TROP1/EPCAM* knockout versus wild-type ES cells under conditions that prevent differentiation (culture over a feeder cell layer, with medium supplemented with leukemia inhibitory factor [LIF])[49] showed distinct patterns of proliferation (Figure 2B). However, LIF can interfere with Trop-1/EpCAM function.[64] Hence, the growth of *TROP1/EPCAM* knockout cell was further assessed in the absence of LIF and of feeder cells. This indicated a lower proliferative capacity of hemizygous *TROP1/EPCAM* ES cells (Figure 2C) versus wt*TROP1/EPCAM*, suggesting a quantitative cell growth response to the *TROP1/EPCAM* gene.

T115 Trop-1/EpCAM is a unique driver of cell growth

Trop molecules drive signaling for growth[19] across distinct normal and transformed cells.[50,65] Among them, L cells were shown to quantitatively respond to the expression of the *TROP1/EPCAM* gene.[66] We transfected L cells with the T115 or M115 Trop-1/EpCAM alleles. Flow cytometry cell sorting[67] selected Trop-1/EpCAM$^+$ cells for parallel expression levels of each Trop-1/EpCAM variant at the cell membrane (Figure 3A, left). Cell growth assays showed that the T115 allele confers hyperproliferative properties, whereas the M115 allele shows little, if any, growth induction capacity (Figure 3A, right). Transfectants were obtained that coexpressed the T115 and M115 Trop-1/EpCAM alleles. Comparative assessment of the T/M versus T/T versus M/M Trop-1/EpCAM alleles showed intermediate levels of cell growth induction for T/M. In other words, we found no evidence for a dominant negative effect of the M115 Trop-1/EpCAM on the T115 allele, but rather a quantitative dependence on T115 Trop-1/EpCAM allele expression levels (Figure 3A, right).

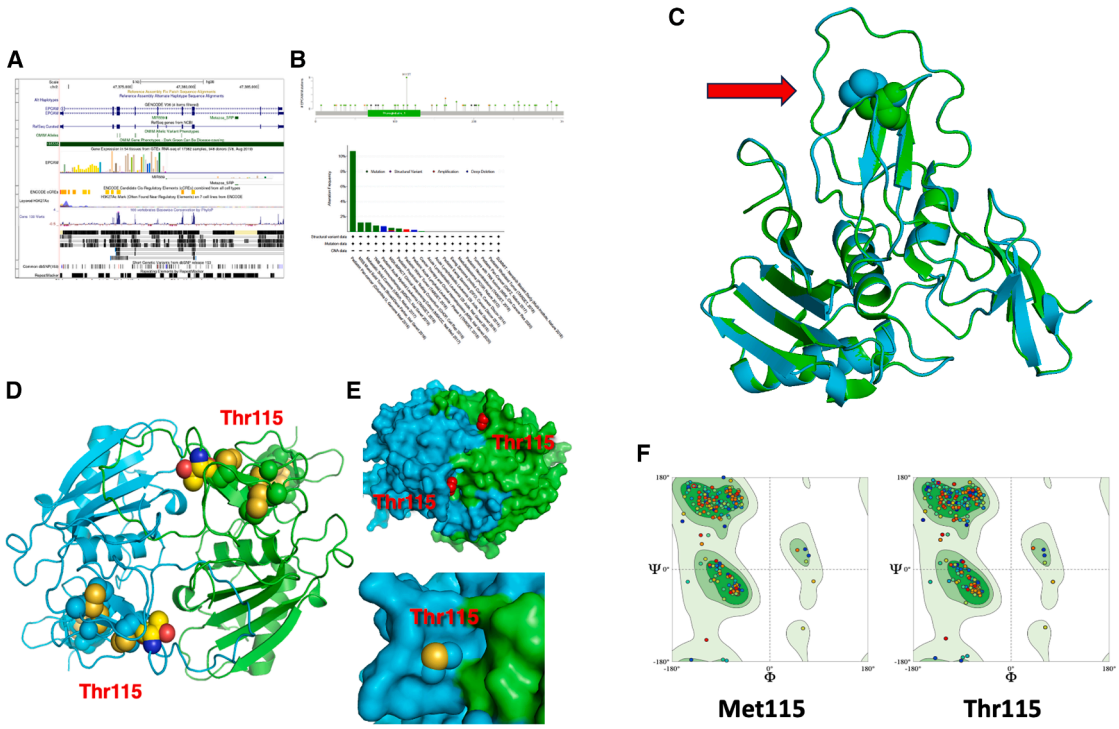

Figure 1. Trop-1/EpCAM M/T variant prevalence and structure/function correlates

(A) Sequence analysis of the *TROP1/EPCAM* gene.

(B) (Top) prevalence of the T115 variant in sequenced cancer genomes. (Bottom) the M115T polymorphism was found to be the main listed variant in the pediatric pan-cancer study (cBioportal; www.cbioportal.org/datasets).

(C and D) Structure of the Trop-1/EpCAM T115 variant. The PDB ID 4mzv was displayed as a dimer as described.[53,54] Trop-1/EpCAM cyan versus green monomers. Red: T115. (C) Cartoon structure representation. (D) (Top) molecular surface representation. Red: T115. (Bottom) zoom-in of the molecular surface. T115 sphere representation.

(E) The T115 Trop-1/EpCAM (4mzv) structure was used as a template to obtain the model structure of the M115 Trop-1/EpCAM.[59,60] The T115 (green) and M115 (cyan) Trop-1/EpCAM variants were superimposed with PyMol (https://www.pymol.org/). Red arrow: T115 (green) and M115 (cyan) space-fill models.

(F) Ramachandran plot analysis of Trop-1/EpCAM T115 and M115 Φ and Ψ peptide bond angles. The Φ and Ψ angles were largely invariant throughout the structure of Trop-1/EpCAM T115 versus M115. Conventionally color-coded residue diagrams are shown. Green shades: allowed regions.

Transgenic T115 Trop-1/EpCAM drives proliferation of CRISPR-Cas9 *TROP1/EPCAM* knockout cancer cells

The human KM12SM colon cancer cells constitutively express Trop-1/EpCAM and quantitatively respond to its growth-induction activity. Thus, we knocked out the endogenous *TROP1/EPCAM* gene in KM12SM cells by CRISPR-Cas9, using two independent frame-shifting single guide RNAs (sgRNAs) targeting distinct regions of the *TROP1/EPCAM* gene (Figures 3B and S2; and STAR Methods). The loss of surface Trop-1/EpCAM protein expression by flow cytometry analysis confirmed the successful ablation of the gene (Figure 3C). We then stably transfected T115 Trop-1/EpCAM (T-mod) or M115 Trop-1/EpCAM (M-mod) expression vectors in the *TROP1/EPCAM*^{KO} KM12SM cells (Figure 3D).

To impede CRISPR-Cas9 from damaging the transduced *TROP1/EPCAM* genes, three silent mutations were introduced in each CRISPR-targeted region of the T-mod and M-mod *TROP1/EPCAM* cDNAs. This rendered the T-mod and M-mod transgenes mismatched and resistant to the CRISPR1 and CRISPR2 complexes that were designed to target the endogenous wt*TROP1/EPCAM* (Figure S2). This strategy allowed us to obtain stable expression of T-mod and M-mod Trop-1/EpCAM in KM12SM/*EPCAM*^{KO} cells. Comparison of the *in vitro* cell proliferation capacity showed that the T115 allele confers hyperproliferative properties, whereas the M115 allele shows little, if any, impact on cancer cell growth (Figure 3E).

Signaling modulation by Trop-1/EpCAM T115 versus M115

Earlier evidence showed that Trop-1/EpCAM and CD9 tightly interact at the plasma membrane of human cancer cells and modulate cell proliferation.[68,69] Here, we found that inhibition of Trop-1/EpCAM expression by CRISPR-Cas9 inactivation of the gene leads to downregulation of CD9 (Figure S3). Notably, re-expression of M115 Trop-1/EpCAM (M-mod) brings CD9 expression back to its original levels. On the other hand, re-expressing T115 Trop-1/EpCAM (T-mod) in the Trop-1/EpCAM knockout cells did not rescue CD9 expression (Figure S3). CD9 has been reported to act as a molecular inhibitor of transformed cell growth.[70] Hence, our findings appear consistent with a role of Trop-1/EpCAM T-mod in inducing cell proliferation also through inhibition of CD9 expression.

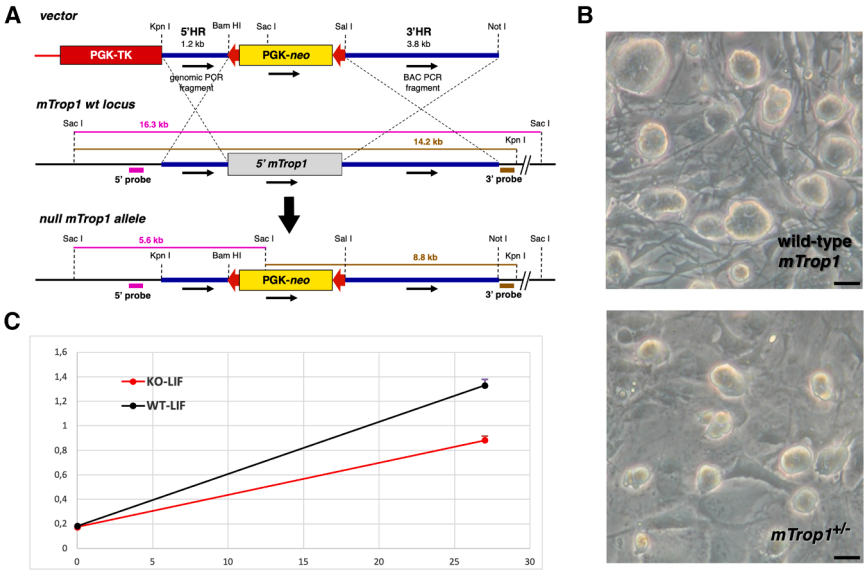

Figure 2. *mTrop1* +/− knockout cells by targeted gene replacement

(A) Scheme of the *mTrop1* inactivation strategy via targeted gene replacement, as adapted from Guerra et al.[49] 5′HR and 3′HR (homology Regions; thick blue lines) indicate the 5′ and 3′ genomic *mTrop1* sequences that were subcloned in the targeting vector, flanking the *mPgk1-neo* resistance cassette (in yellow; red arrows: lox sites). External to the HRs the vector carries the *mPgk1-TK* suicide cassette (in red). Vector-borne *mTrop1* HRs may undergo homologous recombination with the corresponding genomic sequences, replacing the intervening sequence in the *mTrop1* locus (in gray) with the resistance cassette, thus generating a null *mTrop1* allele. Probe position, relevant restriction enzymes, and corresponding DNA fragment lengths are indicated for 5′ (magenta) and 3′ (brown). Southern hybridization analysis. PGK, phosphoglycerate kinase promoter; *neo*, neomycin phosphotransferase gene; TK, thymidine kinase gene.

(B) ES cells were cultured over a feeder layer of mitomycin-C-treated mouse embryonic fibroblast (MEF), and appeared as refractile cell aggregates under phase-contrast microscopy (20× objective). Hemizygous *mTrop1*+/− ES cells reached a lower size of cell aggregates than the *mTrop1* ES cells. Scale bars, 50 μm.

(C) Growth curves in the absence of LIF of wild-type *mTrop1* ES cells (WT-LIF) and of hemizygous *mTrop1*+/− ES cells (knockout [KO]-LIF). KO-LIF showed a lower proliferative capacity than WT-LIF.

Hyperproliferative alveolar repair in T115 Trop-1/EpCAM patients

Autoptic lung specimens from deceased COVID-19 patients were analyzed (Table S1). Histologic findings of acute diffuse alveolar damage (DAD)[51] were seen in all cases, with late phases of DAD being detected in 65% of them. Hyaline membranes were found in 15 out of 20 (75%) cases (Tables S1 and S2). Squamous metaplasia was seen in 4 out of 20 (20%) cases. Capillary microthrombi were present in 7 out of 20 (35%) cases. In 17 of these patients, we were able to evaluate the status of the T115/M115 (M/T) polymorphism: 7 showed an M115 homozygous status (M/M), 1 T115 homozygous status (T/T), and 9 M/T heterozygous status. Due to the low number, the T/T homozygous case was compounded with the 9 M/T heterozygous cases.

Trop-1/EpCAM expression was evaluable in 18 out of 20 autoptic lung specimens. In all cases membrane immunoreactivity for Trop-1/EpCAM was found in DAD areas with AT2 pneumocyte hyperplasia (Figure 4). High, diffuse expression of Trop-1/EpCAM was found in 14 out of 20 cases (70%), in overproliferating AT2 pneumocytes (Figure 4). A larger fraction of AT2 cells expressed Trop-1/EpCAM in M/T patients (67.8% ± 5.4%; mean ± SEM) versus M/M patients (40.9% ± 8.9%) ($p = 0.017$, independent-samples *t* test), consistent with a model of T115 Trop-1/EpCAM as a driver of aberrant, hyperproliferative alveolar repair (Table S1A).

Proliferation rates of epithelial cells were determined by IHC for Ki67 expression in Formalin-Fixed Paraffin-Embedded (FFPE) lung tissues. Ki67 expression profiles in pneumocytes of M/M homozygous and M/T heterozygous patients are shown in Figure 5. The median expression of Ki67 in AT2 pneumocytes in patients with COVID-19 was vastly higher than in controls, indicating hyperproliferative alveolar repair in COVID-19 patients (Mann-Whitney U Test; U value = 0, molecular weight [MW] p = 0.0000014). M/T heterozygous patients showed significantly higher numbers of $Ki67^+$ AT2 pneumocytes than M/M homozygous patients (U value = 4.0, MW $p = 0.04$), consistent with a proliferation driving role of T115 Trop-1/EpCAM.

High expression of Trop-1/EpCAM was found from early stages of injury repair, i.e., in AT2 pneumocyte cell monolayers (Figure 6, left). At later stages, the alveolar space appeared lined by multiple layers of proliferating epithelial cells, which expressed homogeneously high levels of Trop-1/EpCAM at the cell membrane (Figure 6, right).

Hyaline membrane formation was found to correlate with DAD (Figure 7; Table S1). Trop-1/EpCAM positivity was found in all cases with hyaline membrane formation, in all cases with squamous metaplasia and in 67% of cases with capillary microthrombi (Figure 8; Table S1).

As the Trop-1/EpCAM paralog Trop-2 can play parallel functional roles,[19,68,72] for completeness of analysis we investigated Trop-2 expression in lung tissues of COVID-19 patients. Consistent with our model, Trop-2 expression was induced in AT2 pneumocyte hyperplasia in regions of epithelial proliferative repair and in the presence of hyaline membranes. The distribution of Trop-2 expression in AT2 cells was shown to be higher in M/T heterozygous patients (58.0 ± 14.3) compared to M/M homozygous patients (41.0 ± 16.5) (Figure S4), suggesting a coordinated role of Trop molecules in lung responses to the viral infection. Further investigation is required to validate a potential involvement of Trop-2 in AT2 cell hyperplasia in COVID-19 patients.

Hyperproliferation of immune cells of T115 Trop-1/EpCAM COVID-19 patients

Innate immune responses are paramount in mounting an effective early response to SARS-CoV-2 infection, and

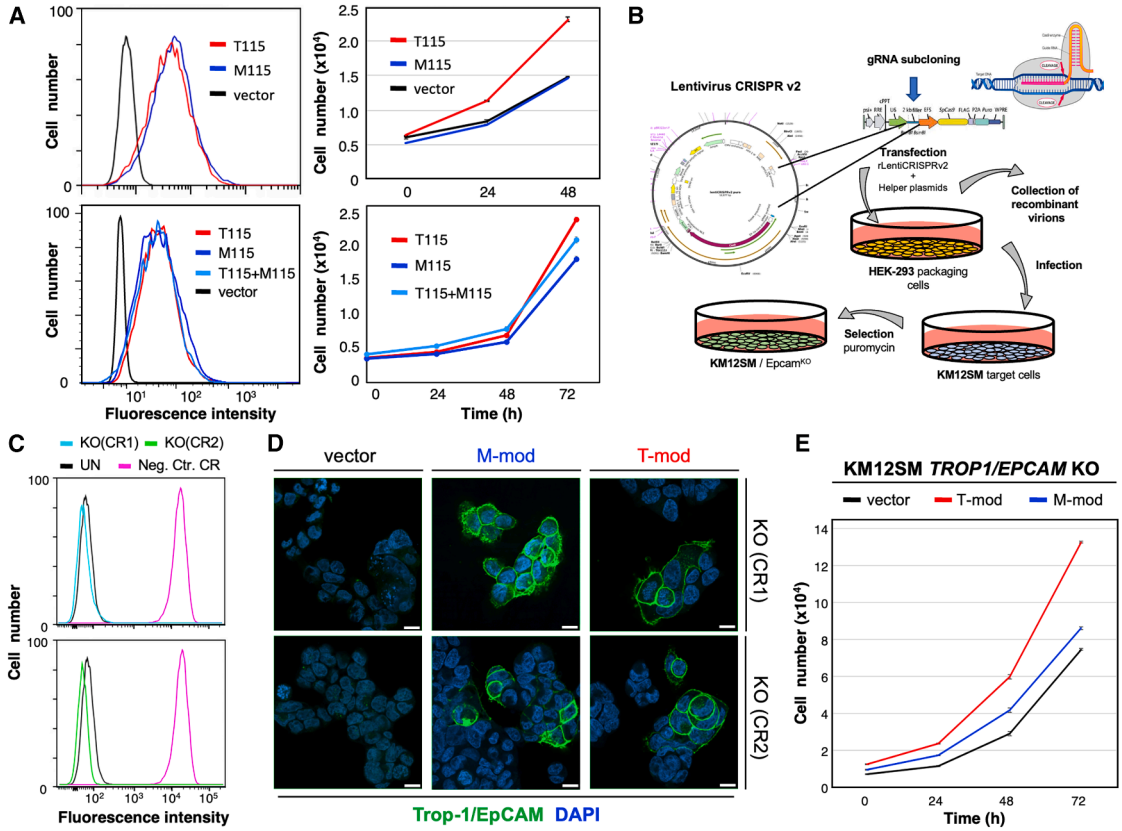

Figure 3. T115 Trop-1/EpCAM induces cell growth

(A) L cell transfectants. (Left) Trop-1/EpCAM flow cytometry profiles of murine fibrosarcoma L cells (devoid of endogenous mTrop-1) transfected with *TROP1/EPCAM* M115 (blue), T115 (red), and M115 + T115 (cyan). (Right) corresponding *in vitro* cell proliferation assay of the L cells transfectants. Data are represented as mean ± SEM of triplicate samples.

(B–E) KM12SM knockout cells. (B) Experimental strategy for generating human cancer cells devoid of Trop-1/EpCAM. Two CRISPR-Cas9 sgRNAs designed to target specific regions (exon 1 and 2) of the human *TROP1/EPCAM* gene were subcloned in the lentiviral vector LentiCRISPRv2. Packaging HEK-293 cells were co-transfected with the recombinant LentiCRISPRv2 and with the helper plasmids pVSVG and psPAX2. Recombinant virions from the tissue culture supernatants were used to infect the KM12SM target cells. Knockout cells were selected with puromycin. (C) Flow cytometry analysis of Trop-1/EpCAM expression in KM12SM cells upon stable inactivation of *TROP1/EPCAM* expression by CRISPR-Cas9. (Black) UN: unstained cells. (Magenta) cells infected with a negative control CRISPR (empty LentiCRISPRv2 virion, neg. ctr. CR). (Cyan) absence of Trop-1/EpCAM expression upon infection of KM12SM with CRISPR1 virions (KO CR1). (Green) absence of Trop-1/EpCAM expression upon infection of KM12SM with CRISPR2 virions (KO CR2). (D) (Green) immunofluorescence/confocal microscopy analysis of Trop-1/EpCAM after transfection of KM12SM knockout cells with the Trop-1/EpCAM variants M-mod or T-mod. (Blue) DAPI counterstaining of cell nuclei. Scale bars, 10 μm. (E) *In vitro* cell proliferation assay of KM12SM knockout cells stably transfected with the *TROP1/EPCAM* M-mod (blue), T-mod (red) variants or empty vector (black). Data are represented as mean ± SEM of triplicate samples.

adaptive immune cells are important for clearing SARS-CoV-2 infection.[73] Consistently with previous findings,[51] inflammatory infiltrates were observed in the lungs of COVID-19 patients in all cases, and were largely composed of macrophages in the alveolar lumen and of lymphocytes in the interstitium, the latter leading to the formation of tertiary lymphoid follicles, as indicators of local hyperimmune response (Figures 9A and 9B).

Consistent with an immunomodulatory role of Trop-1/EpCAM,[74] high expression of Trop-1/EpCAM was shown in intraalveolar macrophages in 79% of the lungs where hyaline membranes were detected (Figure 9A), suggesting an activation role of Trop-1/EpCAM in inflammatory cells, and the association of aberrant epithelial repair with macrophage recruitment and hyperproliferation, associated to tissue hyperinflammation.

Proliferation rates of macrophages in M/M versus M/T COVID-19 patients were analyzed by IHC for Ki67 expression. The median fraction of Ki67$^+$ macrophages in patients with COVID-19 was significantly higher than in control groups (Mann-Whitney U Test; U value = 0, p = 0.000008). Among expressing cases, the median fraction of Ki67$^+$ macrophages was found to be significantly higher in M/T patients versus M/M cases (U value = 0.5, MW p = 0.008) (Figure 9B). Thus, Trop-1/EpCAM T115 patients showed significantly increased proliferation of immune cells, consistent with a pro-inflammatory, proliferation driving role of T115 Trop-1/EpCAM.

As Trop-1/EpCAM modulates the cell-cell adhesive function of E-cadherin[30] and the signaling of β-catenin[49] IHC analysis on FFPE lung tissues was conducted for E-cadherin and β-catenin expression. Inter-membranous E-Cadherin expression was

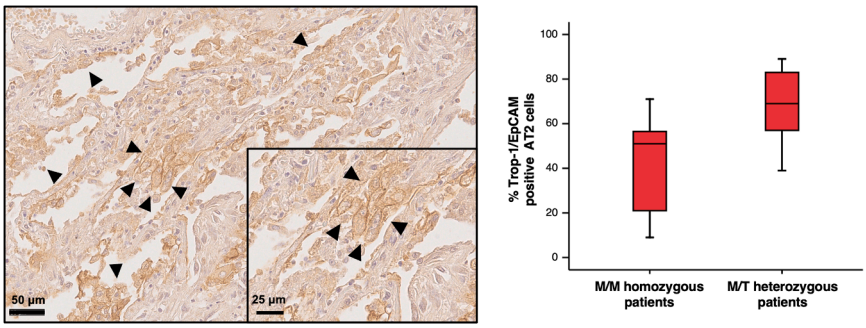

Figure 4. Trop-1/EpCAM expression is induced in pneumocyte hyperplasia

Whole slides from patient samples (Tables S1A and S1B) were systematically examined. Trop-1/EpCAM expression, revealed as described in STAR Methods, was quantified in ten random field spots for each slide, using a 20× objective lens.[71] A 20× objective lens microscopic field corresponds to a surface with a major axis of 1 mm. Statistical analyses were performed as described in STAR Methods. (Left) Diffuse immunostaining for Trop-1/EpCAM in AT2 pneumocyte hyperplasia in COVID-19 patients (arrowheads). Pneumocytes appear enlarged and atypical. Main figure: scale bars, 50 µm; magnified figure: scale bars, 25 µm. (Right) box and whisker diagram of the distribution of Trop-1/EpCAM expression in AT2 pneumocyte hyperplasia. Lung autopsy specimens of deceased COVID-19 patients (n = 18). Upper and lower box borders: 75th and 25th percentile, respectively. Bars: confidence intervals. Horizontal solid line: median value. M/T cases showed up to 2-fold higher expression of Trop-1/EpCAM. A larger fraction of AT2 cells expressed Trop-1/EpCAM in M/T heterozygous patients (67.8% ± 5.4%; mean ± SEM) versus M/M homozygous patients (40.9% ± 8.9%) (p = 0.017, independent-samples t test). These pictures are representative of the analyzed samples.

found in 2 out of 20 cases in endothelial cells with focal expression, in 10 out of 20 cases in ciliated columnar cells (2 cases with focal and 8 cases with diffuse expression) and in 11 out of 20 cases in alveolar epithelial cells (7 cases showed a diffuse staining). Focal patterns of β-catenin expression were rarely detected (2 of 20 cases in endothelial cells; 5 of 20 cases in ciliated columnar cells). In alveolar epithelial cells, β-catenin immunostaining was essentially undetectable (Table S1).

Hyperproliferative alveolar repair generates barriers to oxygen diffusion

COVID-19-induced lung injuries include hyaline membranes, squamous cell hyperplasia and metaplasia, and capillary microthrombi.[1] Our findings indicated broad incidence of tissue repair-induced architectural rearrangements in the lungs of the patients with severe COVID-19 pathology which expressed T115 Trop-1/EpCAM (Figure 10). Normal alveoli lining cells have been optimized through evolution to provide a large surface for gas exchange through thin epithelial layers in close contact with lung capillaries.[75] We thus analyzed the impact of the lung pathological changes on the oxygen diffusion rates in COVID-19 patients.

Gas diffusion through media obeys the Fick's laws.[76] Oxygen diffusion across the alveolar membrane is driven by a pressure gradient Δp between alveolar (100 mmHg) and capillary (40 mmHg) spaces. Diffusion rates are then determined by the oxygen solubility, permeability, and diffusion coefficients (STAR Methods).

As oxygen is ~25 times more soluble in lipids than in water, the limiting factors in oxygen diffusion are the diffusion rates across water layers.[77] To bind hemoglobin in red blood cells (RBCs), oxygen must traverse the alveolar pneumocytes, the capillary walls, the blood plasma (equivalent to a 1 µm-thick unstirred layer of water), and RBC (average thickness 1.6 µm). These processes lead to an average oxygen diffusion rate of 0.2 cm/s.[78] The transit time of RBC in lung capillaries under maximal exercise is 0.25 s. Molecular dynamics simulation shows that an oxygen diffusion rate of 0.2 cm/s allows a limiting ≤95% equilibration of RBC hemoglobin under heavy exercise.[78] As a consequence, pathological changes that occur during the course of acute SARS-CoV-2 infection, via DAD, interstitial edema, capillary microthrombi,[1] are likely to affect oxygen diffusion. However, subsequent injury repair may represent the most serious factor that negatively impacts on lung function, through the formation of hyaline membrane and aberrant alveolar repair by hyperproliferating dysplastic/metaplastic epithelial cells.[79]

As indicated, hyaline membranes were detected in 75% of COVID-19 cases. The thickness of hyaline membranes was systematically measured (n = 154) in representative patient cases. The average thickness was found to be 7.5 ± 0.3 µm (mean ± SEM) (Table S2). As the average thickness of type 1 pneumocytes in normal lungs is 0.36 µm, this is expected to lead to ≥20-fold reduction of oxygen flow in areas containing hyaline membranes.

AT2 pneumocyte hyperplasia was detected in 70% of COVID-19 cases. We systematically assessed the thickness of the epithelial AT2 proliferating cells that substituted virus-damaged AT1 pneumocytes. This showed an increase in the thickness of cell monolayers to 1.5 µm, indicating ≈5-fold longer paths for oxygen diffusion. At subsequent stages, epithelial cells grew to multi-layer aggregates, and the thickness of alveoli-lining membrane went up to 31 µm. This represents a ≈100-fold longer diffusion path for oxygen, with a corresponding reduction of oxygen flow in the affected alveoli (Figure 10). These findings suggested that post-injury repair in COVID-19 patients can lead to vast reduction of the gas-exchange capability of the affected areas.

The alveoli surface area was also severely reduced. The surface area "A" of a sphere is A = $4\pi r^2$, where r is the radius of the sphere. The average radius of an alveolus is around 100 µm,[75] for an average alveolar surface of 125,600 µm^2 (Figure 10). According to measurements in COVID-19 patients, alveolar cavity radii can drop to almost one-half (≈61.5 µm radius), when multi-layered epithelial cells and hyaline membranes are generated by lung injury/lung injury repair (Figure 10). This will then lead to a corresponding severe reduction of the surface area for gas exchanges.

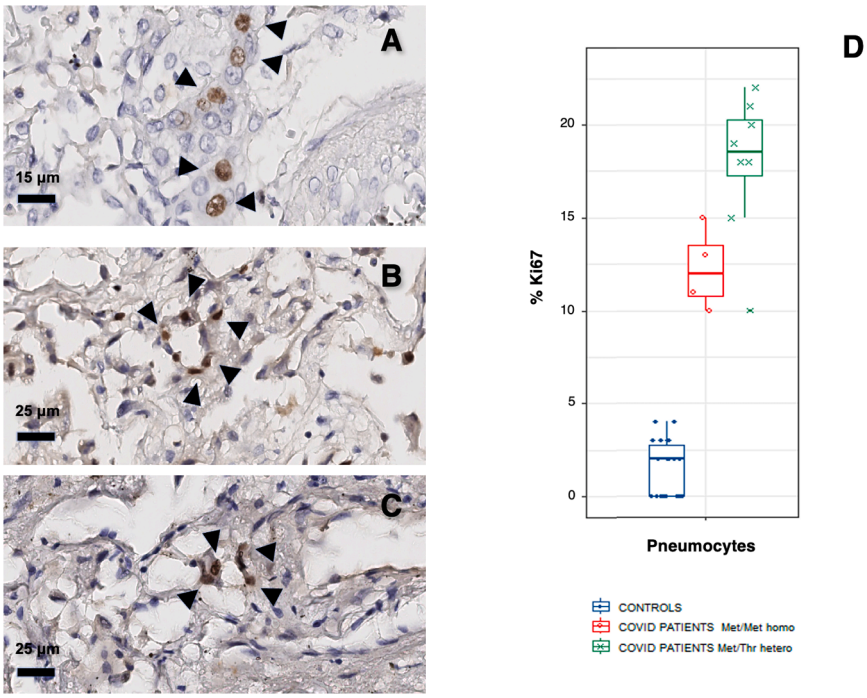

Figure 5. Epithelial cell proliferation in lung lesion repair—Ki67 immunostaining

(A) M/M homozygous.

(B) M/T heterozygous.

(C) T/T homozygous patients. Arrowheads: alveolar type 2 Ki67 positive cells.

(D) Box and whisker diagram of the distribution of percent Ki67 reactivity in pneumocytes in COVID-19 patients according to Trop-1/EpCAM variants: Met/Met (red) or Thr/Met (green). The corresponding distributions in control patients, not affected by COVID-19, are shown in blue. Median macrophage proliferation was 12% in Met/Met patients, 19% in Thr/Met cases, supporting a role in driving hyperinflammation. Upper and lower box borders: 75th and 25th percentile, respectively. Bars: confidence intervals. Horizontal solid line: median value. Dots: individual values. The median expression of Ki67 in AT2 pneumocytes in patients with COVID-19 was higher than in controls (Mann-Whitney U test; U value = 0, MW p = 0.0000014). M/T heterozygous patients showed significantly higher numbers of Ki67^{+} AT2 pneumocytes than M/M homozygous patients (U value = 4.0, MW p = 0.04). These pictures are representative of the analyzed samples.

Scale bars: 15 µm in (A) and 25 µm in (B) and (C). Whole slides from patient samples (Tables S1A and S1B) were systematically examined. Ki67 expression, revealed as described in STAR Methods, was quantified in ten random microscopic field spots for each slide, using a 20× objective lens.[71] A 20× objective lens microscopic field corresponds to a surface with a major axis of 1 mm. Statistical analyses were performed as described in STAR Methods.

DISCUSSION

SARS-CoV-2 lung infection triggers acute lesions and post-acute reactions that severely impair oxygen exchange. However, the underlying molecular processes are poorly understood. Our findings indicated that p.T115 *TROP1/EPCAM* is associated to severe COVID-19 pathology. However, very little information was available on this polymorphism,[55] and M115T was broadly misclassified as a mutation in cancer sequence databanks. In this article we show that the T115 Trop-1/EpCAM is a unique inducer of cell proliferation. This was shown in *TROP1/EPCAM*$^{+/-}$ ES cells and in L cell fibrosarcoma transfectants. CRISPR-Cas9 ablation of the *TROP1/EPCAM* gene in human Trop-1/EpCAM-dependent colon cancer cells, followed by transgenesis with the T115 allele versus the M115 Trop-1/EpCAM allele, formally confirmed the hyperproliferative capacity of T115 Trop-1/EpCAM.

These findings gave us the lead for exploring fundamental determinants of COVID-19 pathology. Lung specimens of deceased COVID-19 patients were analyzed for the prevalence of Trop-1/EpCAM expression and for pathological parameters linked to the T115 allele. Immunohistochemical analysis showed cell membrane expression of Trop-1/EpCAM in essentially all wound-healing AT2 pneumocytes. The fraction of Ki67^{+} proliferating epithelial cells showed a tight correlation with the Thr115 patient phenotype, supporting epithelial hyperproliferation in response to the viral infection as a pathological mechanism for disease severity.

Trop-1/EpCAM expression was found in all cases showing squamous metaplasia, in two-thirds of cases with capillary microthrombi, and in four-fifths of cases with hyaline membrane formation, suggesting additive impact of epithelial cells hyperproliferation with other lesions associated to disease severity. High expression of Trop-1/EpCAM was found from early stages of injury repair, such as in AT2 pneumocyte cell monolayers that substituted virus-damaged AT1 cells. At later stages of injury repair, alveolar spaces appeared lined by multiple layers of proliferating Trop-1/EpCAM^{high} epithelial cells.

Oxygen diffusion in the lungs obeys the Fick's laws[76] and is dependent on oxygen solubility, permeability, and diffusion coefficients. Oxygen is ~25 times more soluble in lipids than in water. Thus, the limiting factors in oxygen diffusion are diffusion rates across water layers.[77] Alveolar repair by epithelial cells appeared to impose a serious limit to oxygen diffusion. Dysplastic/metaplastic AT2 proliferating cells, that substituted normal type 1 pneumocytes,[79] increased cell monolayer thickness from 0.36 µm to 1.5 µm, for 5-fold longer paths for oxygen diffusion. The thickness of epithelial cell membranes that lined alveolar spaces went subsequently up to ≥30 µm in multi-layered regions, for a ≈100-fold longer oxygen diffusion path, with a corresponding reduction of oxygen flow in the affected alveoli. The alveoli surface area also appeared severely reduced, when multiple layers of epithelial cells were generated by hyperproliferative repair of lung injuries. Formation of hyaline membranes was detected in 75% of COVID-19 cases. As the average thickness of hyaline membranes was 7.5 µm, the presence of hyaline membranes was projected to lead to additional ≥20-fold reduction of oxygen flow versus normal lungs.

Trop-1/EpCAM can additionally exert an immunomodulatory role,[74] via increase of the migratory capacity of

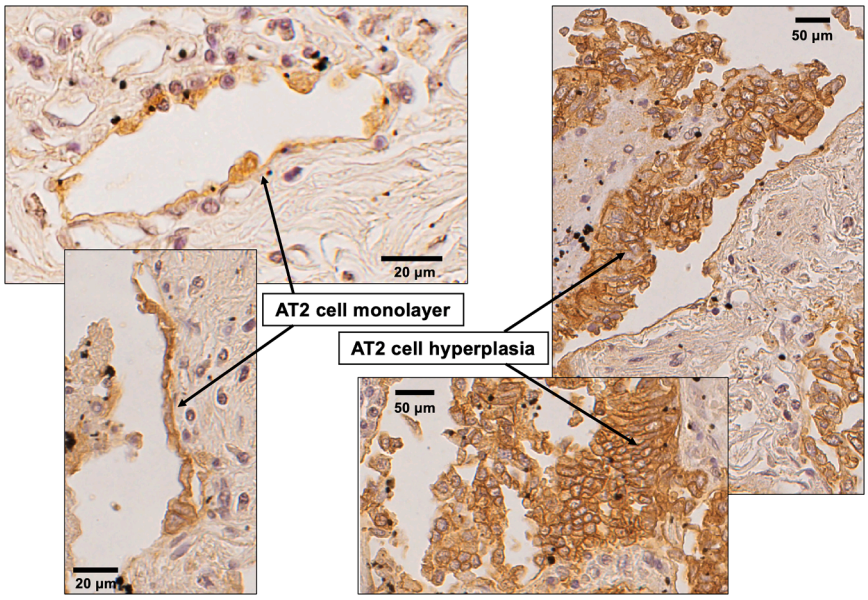

Figure 6. High immunostaining for Trop-1/EpCAM in AT2 pneumocyte hyperplasia (arrowheads)

(Left): Trop-1/EpCAM positive cell monolayers in samples from Trop-1/EpCAM M115 homozygous patients. Scale bars, 20 μm. (Right): Trop-1/EpCAM positive multi-layered hyperplastic cells in samples from Trop-1/EpCAM M115/T115 heterozygous patients. Scale bars, 50 μm. These pictures are representative of the analyzed samples.

inflammatory cells and of tolerogenic functions.[80–83] Induction of expression of Trop-1/EpCAM was revealed in intraalveolar macrophages and was associated with formation of tertiary lymphoid follicles in the lung interstitium, consistent with a localized hyperactive immune response. Thus, our findings support the association of Trop-1/EpCAM with hyperinflammatory processes that lead to DAD, intestitial edema, capillary microthrombi, and hyaline membrane formation, adding to the severity of reduction of oxygen exchange rates.

Recent findings have identified a role for fibroblast-mediated pathological mechanisms as triggered by injury repair in the lungs. After severe injury, alveolar fibroblasts promote a competition between airway stem cells versus alveolar stem cells.[79] As a consequence, dysplastic airway-derived Krt5^{+} basal epithelial cells invade the alveolus during wound repair. Notch activation, which represses Wnt/fibroblast growth factor (FGF) in the injured alveolus, then establishes a non-resolving niche, which stably maintains a dysplastic alveolar phenotype.[79] Healed lesions thus largely fail to recover to a physiological state, thereby hindering the recovery of normal gas permeability in seriously affected patients.

The T115 Trop-1/EpCAM polymorphism was shown to be an independent risk factor for disease severity after adjusting for competing risks. In other words, in a population whereby other risk factors, e.g., age, sex, and pre-existing pathologies, are taken into account, the abnormal hyperproliferative repair in T115 Trop-1/EpCAM patients independently adds a disease risk and associates to severe clinical outcomes, via a reduction of oxygen diffusion rates in affected alveoli. These findings suggest that T115 Trop-1/EpCAM genetic determination may help stratifying patients into dichotomous cohorts with distinctly different COVID-19 disease risk. Trop-1/EpCAM-focused therapeutic interventions may be explored in T115 cases.[84,85]

Limitations of the study

Main limitations of the study are the low numbers of COVID-19 autoptic samples in patient subgroups. An additional limitation of the study is the lack of *in vivo* validation of the reduction of oxygen diffusion rates in the COVID-19 patients analyzed, as the study was based on deceased patients and on autoptic samples. Finally, additional work is required to show that T115 Trop-1/EpCAM-associated pro-inflammatory changes play a role in COVID-19 disease severity.

RESOURCE AVAILABILITY

Lead contact

Further information and requests for resources and reagents should be directed to and will be fulfilled by the lead contact, Saverio Alberti (salberti@unime.it).

Materials availability

The reagents generated in this study will be made available on request, but we may require a payment and/or a completed materials transfer agreement if there is potential for commercial application.

Data and code availability

- All data produced for this manuscript are available from the lead contact upon reasonable request. GEN-COVID data are available for sharing through the COVID-19 dedicated section (http://nigdb.cineca.it), within the Network for Italian Genome (http://www.nig.cineca.it). The data and samples referenced here are housed in the GEN-COVID Patient Registry and the GEN-COVID Biobank and are available for consultation.
- This paper does not report original code. Any additional information required to reanalyze the data reported in this paper is available from the corresponding author upon request.

Institutional review board statement

All the enrolled subjects were adults (aged ≥18 years) and either they, or their legally authorized representatives, provided informed consent for participation. Specimens were provided by the COVID-19 Biobank of Siena, which is part of the Genetic Biobank of Siena, member of BBMRI-IT, Telethon Network of Genetic Biobanks (project no. GTB18001), and the EuroBioBank. This study is part of the GEN-COVID Multicenter Study, https://sites.google.com/dbm.unisi.it/gen-covid, the Italian multicenter study aimed at identifying the COVID-19 host genetic bases. The GEN-COVID Multicenter Study was approved by the University Hospital (Azienda ospedaliero-universitaria Sense) Ethical Review Board, Siena, Italy (Prot n. 16917, dated March 16, 2020) and by the local IRBs of all the recruiting hospitals involved.

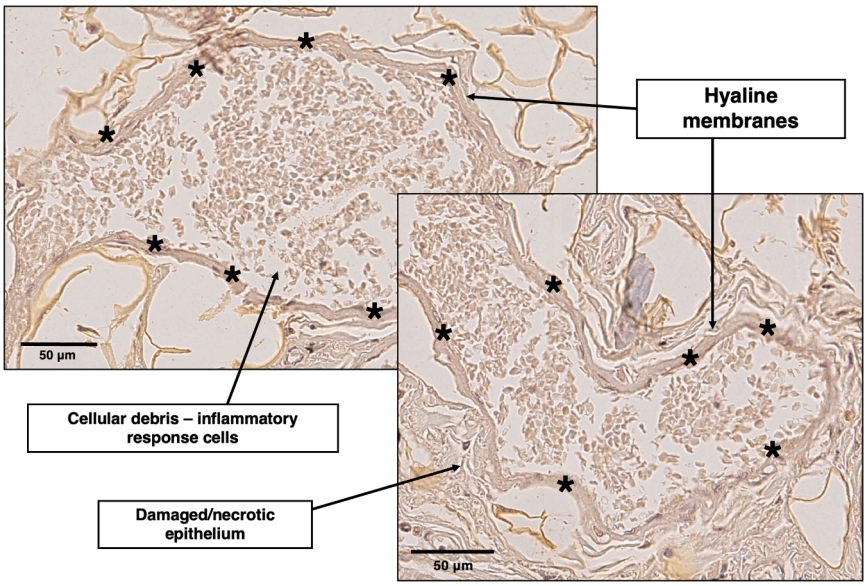

Figure 7. Hyaline membranes are present in regions with diffuse lung alveolar damage

Histologic findings of acute diffuse alveolar damage (DAD) were seen in all COVID-19 cases, with late phases of DAD seen in 65% of patients. Hyaline membranes were seen in 15 out of 20 (75%) of patients (Table S2). (Left) sample from a Trop-1/EpCAM M115 homozygous patient. (Right) sample from a Trop-1/EpCAM M115/T115 heterozygous patient. Scale bars, 50 μm. These pictures are representative of the analyzed samples.

ACKNOWLEDGMENTS

This study is part of the GEN-COVID Multicenter Study (https://sites.google.com/dbm.unisi.it/gen-covid), the Italian multicenter study aimed at identifying the COVID-19 host genetic bases. Specimens were provided by the COVID-19 Biobank of Siena, which is part of the Genetic Biobank of Siena, member of BBMRI-IT, Telethon Network of Genetic Biobanks (project no. GTB18001), the EuroBioBank, and RD-Connect. All authors of this paper are members of European Reference Network on rare respiratory diseases ERN-LUNG. We thank the CINECA consortium for providing computational resources and the Network for Italian Genomes (NIG; http://www.nig.cineca.it) for its support. We thank private donors for the support provided to A.R. (Department of Medical Biotechnologies, University of Siena) for the COVID-19 host genetics research project (D.L. n.18 of March 17, 2020). We also thank the COVID-19 Host Genetics Initiative (https://www.COVID-19hg.org/), MIUR project 'Dipartimenti di Eccellenza 2018–2020 to the Department of Medical Biotechnologies University of Siena, Italy, and 'Bando Ricerca COVID-19 Toscana' project to Azienda Ospedaliero-Universitaria Senese. We thank the Intesa San Paolo for the 2020 charity fund dedicated to the project N B/2020/0119 "Identificazione delle basi genetiche determinanti la variabilità clinica della risposta a COVID-19 nella popolazione italiana". The Italian Ministry of University and Research for funding within the "Bando FISR 2020" in COVID-19 for the project "Editing dell'RNA contro il Sars-CoV-2: hackerare il virus per identificare bersagli molecolari e attenuare l'infezione - HACKTHECOV)" and the Istituto Buddista Italiano Soka Gakkai for funding the project "PAT-COVID: Host genetics and pathogenetic mechanisms of COVID-19" (ID n. 2020-2016_RIC_3). We thank EU project H2020-SC1-FA-DTS-2018-2020, entitled "International consortium for integrative genomics prediction (INTERVENE)" – grant agreement no. 101016775. We gratefully acknowledge the support of the Fondazione Compagnia di San Paolo (grant no. 2489IT), the Ministry of the University and Research (MIUR, Italy) (SCN_00558), and the Ministry of Development Italy (MI01_00424), Region Abruzzo (POR FESR 2007–2013: Activity 1.1.1 line B), the Italian Association for Cancer Research. Generous support was also received from private donations by Mrs. Maurizio Traglio, Enzo Cattaneo, and Alberto Borella. Graphical abstract created in BioRender, E.G. (2026) https://BioRender.com/p4mbqap.

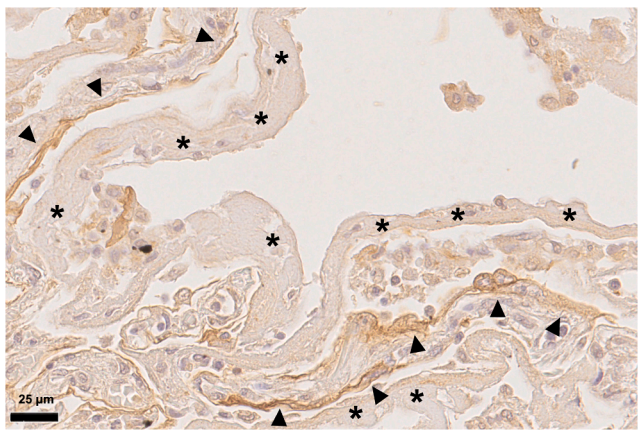

Figure 8. Hyaline membranes and Trop-1/EpCAM-expressing type 2 pneumocytes are present in most COVID-19 patients

*: Hyaline membranes. Correlated immunostaining for Trop-1/EpCAM is present in AT2 pneumocytes (brown areas, arrowheads). Sample from a Trop-1/EpCAM M115/T115 heterozygous patient. Scale bars, 25 μm. The presented picture is representative of the analyzed samples of the case series analyzed.

AUTHOR CONTRIBUTIONS

C.F., M.T., R.L., and S.A., study concept, designing and drafting of the manuscript; M.B., data acquisition and drafting of the manuscript; S.M., G.R., and B.T., data analysis and interpretation; G.B., statistical analysis; C.A., V.G., C.P., A.M., and F.M.P., image analysis and data acquisition and validation; L.B., experimental lung function assessment; N.L.F., E.G., M.C., and L.P., *mTrop1/mEpcam* gene knockout, CRISPR-Cas9 *TROP1/EPCAM* gene inactivation and transgenesis experiments, and cell proliferation assays in cell culture and in patient samples; N.f.I.G. and G.-C.M.S. consortia, machine learning, training, and application and exome sequencing data analysis; A.R., S.A., E.B., and C.B., study supervision, data analysis and interpretation and critical revision of the manuscript for important intellectual content. All authors read and approved the final manuscript.

DECLARATION OF INTERESTS

The authors declare no competing interests.

STAR★METHODS

Detailed methods are provided in the online version of this paper and include the following:

- KEY RESOURCES TABLE

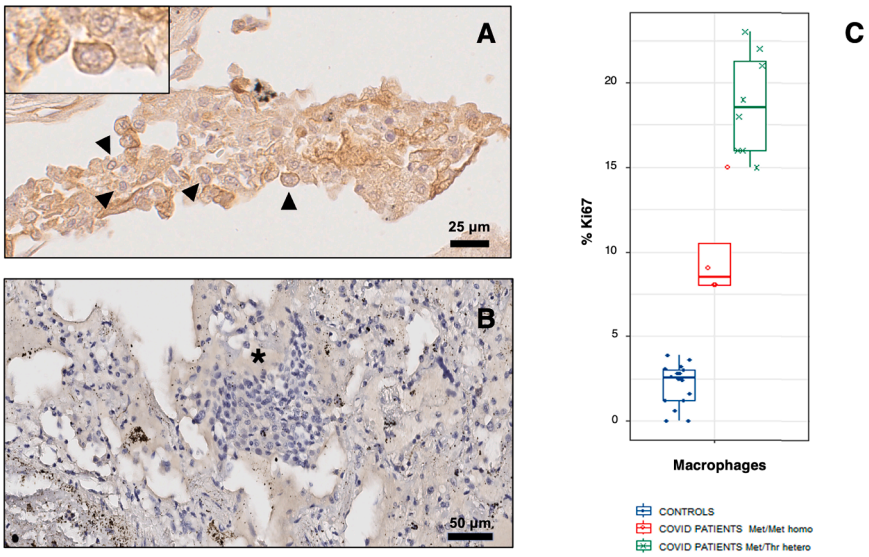

Figure 9. Inflammatory cell responses in COVID-19 patient lungs

(A) Immunostaining for Trop-1/EpCAM expression in intraalveolar macrophages (arrowheads). Scale bars, 25 µm. (Inset) magnified macrophage (bottom arrow) with prevalent membrane localization of Trop-1/EpCAM.

(B) *: tertiary lymphoid follicle developing in the hyperinflammed lung of an MT patient. Scale bars, 50 µm.

(C) Box and whisker diagram of the distribution of Ki67 reactivity in macrophages in COVID-19 patients according to Trop-1/EpCAM variants. Met/Met (red), Thr/Met (green). The corresponding distributions in control patients, not affected by COVID-19, are shown in blue. Median macrophage proliferation was 7% in Met/Met patients, 17.5% in Thr/Met cases. Upper and lower box borders: 75th and 25th percentile, respectively. Bars: confidence intervals. Horizontal solid line: median value. Dots: individual values. The median fraction of Ki67^{+} macrophages in patients with COVID-19 was significantly higher than in control groups (Mann-Whitney U Test; U value = 0, p = 0.000008). The median fraction of Ki67^{+} macrophages was significantly higher in M/T heterozygous patients versus M/M homozygous cases (U value = 0.5, MW p = 0.008). These pictures are representative of the analyzed samples.

Whole slides from patient samples (Tables S1A and S2B) were systematically examined. Trop-1/EpCAM expression in macrophages was revealed as described in STAR Methods and was quantified in ten random microscopic field spots for each slide, using a 20× objective lens.[71] A 20× objective lens microscopic field corresponds to a surface with a major axis of 1 mm. Statistical analyses were performed as described in STAR Methods.

SUPPLEMENTAL INFORMATION

Supplemental information can be found online at https://doi.org/10.1016/j.isci.2026.117361.

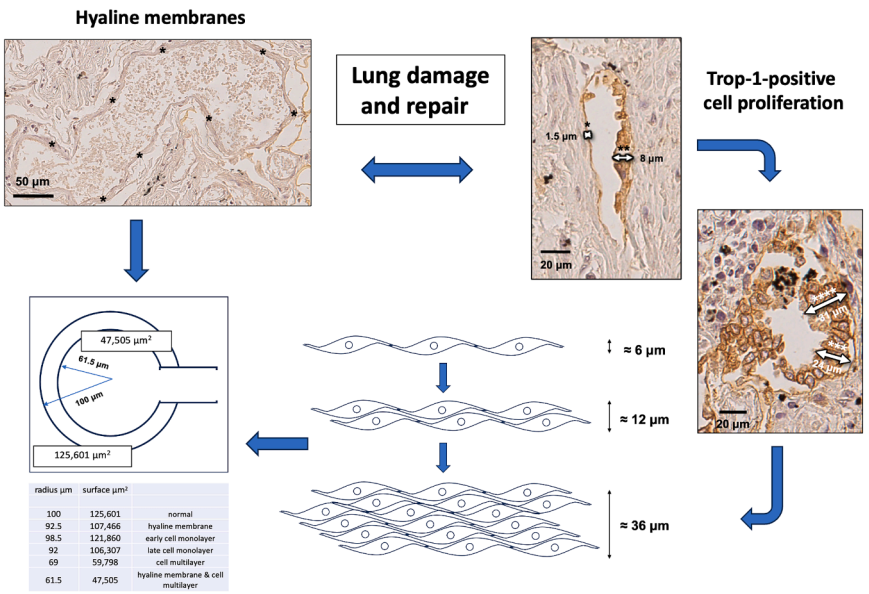

Figure 10. Oxygen diffusion upon lung injury and repair

The cartoon outlines the main damage and repair mechanisms in the lung post-acute SARS-CoV-2 infection. (Upper left) formation of hyaline membranes. (Right) AT2 pneumocyte hyperplasia. Immunohistochemical staining for Trop-1/EpCAM. *: 1–5 µm epithelium thickness; **: 6–15 µm; ***: 16–26 µm; ****: ≥27 µm. (Lower left) model of a lung alveolus radius and overall surface area under normal conditions and upon pathological changes.[75] Blue arrows indicate the progression path of the disease. Scale bars: 50 µm in the upper left picture and 20 µm in the right pictures.

Received: July 9, 2025
Revised: March 13, 2026
Accepted: August 12, 2026

REFERENCES

1. Wiersinga, W.J., Rhodes, A., Cheng, A.C., Peacock, S.J., and Prescott, H.C. (2020). Pathophysiology, Transmission, Diagnosis, and Treatment of Coronavirus Disease 2019 (COVID-19): A Review. JAMA *324*, 782–793. https://doi.org/10.1001/jama.2020.12839.

2. Wu, C., Chen, X., Cai, Y., Xia, J., Zhou, X., Xu, S., Huang, H., Zhang, L., Zhou, X., Du, C., et al. (2020). Risk Factors Associated With Acute Respiratory Distress Syndrome and Death in Patients With Coronavirus Disease 2019 Pneumonia in Wuhan, China. JAMA Intern. Med. *180*, 934–943. https://doi.org/10.1001/jamainternmed.2020.0994.

3. Grasselli, G., Greco, M., Zanella, A., Albano, G., Antonelli, M., Bellani, G., Bonanomi, E., Cabrini, L., Carlesso, E., Castelli, G., et al. (2020). Risk Factors Associated With Mortality Among Patients With COVID-19 in Intensive Care Units in Lombardy, Italy. JAMA Intern. Med. *180*, 1345–1355. https://doi.org/10.1001/jamainternmed.2020.3539.

4. Severe Covid-19 GWAS Group; Ellinghaus, D., Degenhardt, F., Bujanda, L., Buti, M., Albillos, A., Invernizzi, P., Fernández, J., Prati, D., Baselli, G., et al. (2020). Genomewide Association Study of Severe Covid-19 with Respiratory Failure. N. Engl. J. Med. *383*, 1522–1534. https://doi.org/10.1056/NEJMoa2020283.

5. Pairo-Castineira, E., Clohisey, S., Klaric, L., Bretherick, A.D., Rawlik, K., Pasko, D., Walker, S., Parkinson, N., Fourman, M.H., Russell, C.D., et al. (2021). Genetic mechanisms of critical illness in COVID-19. Nature *591*, 92–98. https://doi.org/10.1038/s41586-020-03065-y.

6. Kosmicki, J.A., Horowitz, J.E., Banerjee, N., Lanche, R., Marcketta, A., Maxwell, E., Bai, X., Sun, D., Backman, J.D., Sharma, D., et al. (2021). Pan-ancestry exome-wide association analyses of COVID-19 outcomes in 586,157 individuals. Am. J. Hum. Genet. *108*, 1350–1355. https://doi.org/10.1016/j.ajhg.2021.05.017.

7. Niemi, M.E.K., Karjalainen, J., Liao, R.G., Neale, B.M., Daly, M., Ganna, A., Pathak, G.A., Andrews, S.J., Kanai, M., Veerapen, K., et al. (2021). Mapping the human genetic architecture of COVID-19. Nature *600*, 472–477. https://doi.org/10.1038/s41586-021-03767-x.

8. Kousathanas, A., Pairo-Castineira, E., Rawlik, K., Stuckey, A., Odhams, C.A., Walker, S., Russell, C.D., Malinauskas, T., Wu, Y., Millar, J., et al. (2022). Whole-genome sequencing reveals host factors underlying critical COVID-19. Nature *607*, 97–103. https://doi.org/10.1038/s41586-022-04576-6.

9. Zhang, Q., Bastard, P., Liu, Z., Le Pen, J., Moncada-Velez, M., Chen, J., Ogishi, M., Sabli, I.K.D., Hodeib, S., Korol, C., et al. (2020). Inborn errors of type I IFN immunity in patients with life-threatening COVID-19. Science *370*, eabd4570. https://doi.org/10.1126/science.abd4570.

10. van der Made, C.I., Simons, A., Schuurs-Hoeijmakers, J., van den Heuvel, G., Mantere, T., Kersten, S., van Deuren, R.C., Steehouwer, M., van Reijmersdal, S.V., Jaeger, M., et al. (2020). Presence of Genetic Variants Among Young Men With Severe COVID-19. JAMA *324*, 663–673. https://doi.org/10.1001/jama.2020.13719.

11. Fallerini, C., Daga, S., Mantovani, S., Benetti, E., Picchiotti, N., Francisci, D., Paciosi, F., Schiaroli, E., Baldassarri, M., Fava, F., et al. (2021). Association of Toll-like receptor 7 variants with life-threatening COVID-19 disease in males: findings from a nested case-control study. eLife *10*, e67569. https://doi.org/10.7554/eLife.67569.

12. Solanich, X., Vargas-Parra, G., van der Made, C.I., Simons, A., Schuurs-Hoeijmakers, J., Antolí, A., Del Valle, J., Rocamora-Blanch, G., Setién, F., Esteller, M., et al. (2021). Genetic Screening for TLR7 Variants in Young and Previously Healthy Men With Severe COVID-19. Front. Immunol. *12*, 719115. https://doi.org/10.3389/fimmu.2021.719115.

13. Baldassarri, M., Picchiotti, N., Fava, F., Fallerini, C., Benetti, E., Daga, S., Valentino, F., Doddato, G., Furini, S., Giliberti, A., et al. (2021). Shorter androgen receptor polyQ alleles protect against life-threatening COVID-19 disease in European males. EBioMedicine *65*, 103246. https://doi.org/10.1016/j.ebiom.2021.103246.

14. Croci, S., Venneri, M.A., Mantovani, S., Fallerini, C., Benetti, E., Picchiotti, N., Campolo, F., Imperatore, F., Palmieri, M., Daga, S., et al. (2022). The polymorphism L412F in TLR3 inhibits autophagy and is a marker of severe COVID-19 in males. Autophagy *18*, 1662–1672. https://doi.org/10.1080/15548627.2021.1995152.

15. Fallerini, C., Daga, S., Benetti, E., Picchiotti, N., Zguro, K., Catapano, F., Baroni, V., Lanini, S., Bucalossi, A., Marotta, G., et al. (2021). SELP Asp603Asn and severe thrombosis in COVID-19 males. J. Hematol. Oncol. *14*, 123. https://doi.org/10.1186/s13045-021-01136-9.

16. Mantovani, S., Daga, S., Fallerini, C., Baldassarri, M., Benetti, E., Picchiotti, N., Fava, F., Gallì, A., Zibellini, S., Bruttini, M., et al. (2022). Rare variants in Toll-like receptor 7 results in functional impairment and downregulation of cytokine-mediated signaling in COVID-19 patients. Genes Immun. *23*, 51–56. https://doi.org/10.1038/s41435-021-00157-1.

17. Baldassarri, M., Fava, F., Fallerini, C., Daga, S., Benetti, E., Zguro, K., Amitrano, S., Valentino, F., Doddato, G., Giliberti, A., et al. (2021). Severe COVID-19 in Hospitalized Carriers of Single CFTR Pathogenic Variants. J. Pers. Med. *11*, 558. https://doi.org/10.3390/jpm11060558.

18. Baldassarri, M., Zguro, K., Tomati, V., Pastorino, C., Fava, F., Croci, S., Bruttini, M., Picchiotti, N., Furini, S., Pedemonte, N., et al. (2022). Gain- and Loss-of-Function CFTR Alleles Are Associated with COVID-19 Clinical Outcomes. Cells *11*, 4096. https://doi.org/10.3390/cells11244096.

19. Zanna, P., Trerotola, M., Vacca, G., Bonasera, V., Palombo, B., Guerra, E., Rossi, C., Lattanzio, R., Piantelli, M., and Alberti, S. (2007). Trop-1 are conserved growth stimulatory molecules that mark early stages of tumor progression. Cancer *110*, 452–464. https://doi.org/10.1002/cncr.22785.

20. Strnad, J., Hamilton, A.E., Beavers, L.S., Gamboa, G.C., Apelgren, L.D., Taber, L.D., Sportsman, J.R., Bumol, T.F., Sharp, J.D., and Gadski, R.A. (1989). Molecular cloning and characterization of a human adenocarcinoma/epithelial cell surface antigen complementary DNA. Cancer Res. *49*, 314–317.

21. Ripani, E., Sacchetti, A., Corda, D., and Alberti, S. (1998). Human Trop-2 is a tumor-associated calcium signal transducer. Int. J. Cancer *76*, 671–676. https://doi.org/10.1002/(sici)1097-0215(19980529)76:5<671::aid-ijc10>3.0.co;2-7.

22. Balzar, M., Briaire-de Bruijn, I.H., Rees-Bakker, H.A., Prins, F.A., Helfrich, W., de Leij, L., Riethmüller, G., Alberti, S., Warnaar, S.O., Fleuren, G.J., and Litvinov, S.V. (2001). Epidermal growth factor-like repeats mediate lateral and reciprocal interactions of Ep-CAM molecules in homophilic adhesions. Mol. Cell Biol. *21*, 2570–2580. https://doi.org/10.1128/MCB.21.7.2570-2580.2001.

23. Picchiotti, N., Benetti, E., Fallerini, C., Daga, S., Baldassarri, M., Fava, F., Zguro, K., Valentino, F., Doddato, G., Giliberti, A., et al. (2021). Post-Mendelian Genetic Model in COVID-19. Cardiol. Cardiovasc. Med. *05*, 673–694. https://doi.org/10.26502/fccm.92920232.

24. Fallerini, C., Picchiotti, N., Baldassarri, M., Zguro, K., Daga, S., Fava, F., Benetti, E., Amitrano, S., Bruttini, M., Palmieri, M., et al. (2022). Common, low-frequency, rare, and ultra-rare coding variants contribute to COVID-19 severity. Hum. Genet. *141*, 147–173. https://doi.org/10.1007/s00439-021-02397-7.

25. Calabrese, G., Crescenzi, C., Morizio, E., Palka, G., Guerra, E., and Alberti, S. (2001). Assignment of TACSTD1 (alias TROP1, M4S1) to human chromosome 2p21 and refinement of mapping of TACSTD2 (alias TROP2, M1S1) to human chromosome 1p32 by in situ hybridization. Cytogenet. Cell Genet. *92*, 164–165. https://doi.org/10.1159/000056891.

26. Aplin, A.E., Howe, A.K., and Juliano, R.L. (1999). Cell adhesion molecules, signal transduction and cell growth. Curr. Opin. Cell Biol. *11*, 737–744. https://doi.org/10.1016/s0955-0674(99)00045-9.

27. Litvinov, S.V., Velders, M.P., Bakker, H.A., Fleuren, G.J., and Warnaar, S.O. (1994). Ep-CAM: a human epithelial antigen is a homophilic cell-cell adhesion molecule. J. Cell Biol. *125*, 437–446. https://doi.org/10.1083/jcb.125.2.437.

28. Tsaktanis, T., Kremling, H., Pavšič, M., von Stackelberg, R., Mack, B., Fukumori, A., Steiner, H., Vielmuth, F., Spindler, V., Huang, Z., et al. (2015). Cleavage and cell adhesion properties of human epithelial cell adhesion molecule (HEPCAM). J. Biol. Chem. *290*, 24574–24591. https://doi.org/10.1074/jbc.M115.662700.

29. Gaber, A., Kim, S.J., Kaake, R.M., Benčina, M., Krogan, N., Šali, A., Pavšič, M., and Lenarčič, B. (2018). EpCAM homo-oligomerization is not the basis for its role in cell-cell adhesion. Sci. Rep. *8*, 13269. https://doi.org/10.1038/s41598-018-31482-7.

30. Litvinov, S.V., Balzar, M., Winter, M.J., Bakker, H.A., Briaire-de Bruijn, I.H., Prins, F., Fleuren, G.J., and Warnaar, S.O. (1997). Epithelial cell adhesion molecule (Ep-CAM) modulates cell-cell interactions mediated by classic cadherins. J. Cell Biol. *139*, 1337–1348. https://doi.org/10.1083/jcb.139.5.1337.

31. Schön, M.P., Schön, M., Klein, C.E., Blume, U., Bisson, S., and Orfanos, C.E. (1994). Carcinoma-associated 38-kD membrane glycoprotein MH 99/KS 1/4 is related to proliferation and age of transformed epithelial cell lines. J. Invest. Dermatol. *102*, 987–991. https://doi.org/10.1111/1523-1747.ep12384258.

32. Klein, C.E., Hartmann, B., Schön, M.P., Weber, L., and Alberti, S. (1990). Expression of 38-kD cell-surface glycoprotein in transformed human keratinocyte cell lines, basal cell carcinomas, and epithelial germs. J. Invest. Dermatol. *95*, 74–82. https://doi.org/10.1111/1523-1747.ep12873988.

33. Cirulli, V., Crisa, L., Beattie, G.M., Mally, M.I., Lopez, A.D., Fannon, A., Ptasznik, A., Inverardi, L., Ricordi, C., Deerinck, T., et al. (1998). KSA antigen Ep-CAM mediates cell-cell adhesion of pancreatic epithelial cells: morphoregulatory roles in pancreatic islet development. J. Cell Biol. *140*, 1519–1534. https://doi.org/10.1083/jcb.140.6.1519.

34. de Boer, C.J., van Krieken, J.H., Janssen-van Rhijn, C.M., and Litvinov, S.V. (1999). Expression of Ep-CAM in normal, regenerating, metaplastic, and neoplastic liver. J. Pathol. *188*, 201–206. https://doi.org/10.1002/(SICI)1096-9896(199906)188:2<201::AID-PATH339>3.0.CO;2-8.

35. Stingl, J., Eaves, C.J., Kuusk, U., and Emerman, J.T. (1998). Phenotypic and functional characterization in vitro of a multipotent epithelial cell present in the normal adult human breast. Differentiation *63*, 201–213. https://doi.org/10.1111/j.1432-0436.1998.00201.x.

36. Anderson, R., Schaible, K., Heasman, J., and Wylie, C. (1999). Expression of the homophilic adhesion molecule, Ep-CAM, in the mammalian germ line. J. Reprod. Fertil. *116*, 379–384. https://doi.org/10.1530/jrf.0.1160379.

37. Lammers, R., Giesert, C., Grünebach, F., Marxer, A., Vogel, W., and Bühring, H.J. (2002). Monoclonal antibody 9C4 recognizes epithelial cellular adhesion molecule, a cell surface antigen expressed in early steps of erythropoiesis. Exp. Hematol. *30*, 537–545. https://doi.org/10.1016/s0301-472x(02)00798-1.

38. Gastl, G., Spizzo, G., Obrist, P., Dünser, M., and Mikuz, G. (2000). Ep-CAM overexpression in breast cancer as a predictor of survival. Lancet *356*, 1981–1982. https://doi.org/10.1016/S0140-6736(00)03312-2.

39. Beverley, P.C., Olabiran, Y., Ledermann, J.A., Bobrow, L.G., and Souhami, R.L. (1991). Results of the central data analysis. Br. J. Cancer Suppl. *14*, 10–19.

40. Al-Hajj, M., Wicha, M.S., Benito-Hernandez, A., Morrison, S.J., and Clarke, M.F. (2003). Prospective identification of tumorigenic breast cancer cells. Proc. Natl. Acad. Sci. USA *100*, 3983–3988. https://doi.org/10.1073/pnas.0530291100.

41. Schön, M.P., Schön, M., Mattes, M.J., Stein, R., Weber, L., Alberti, S., and Klein, C.E. (1993). Biochemical and immunological characterization of the human carcinoma-associated antigen MH 99/KS 1/4. Int. J. Cancer *55*, 988–995. https://doi.org/10.1002/ijc.2910550619.

42. Wu, C.J., Feng, X., Lu, M., Morimura, S., and Udey, M.C. (2017). Matriptase-mediated cleavage of EpCAM destabilizes claudins and dysregulates intestinal epithelial homeostasis. J. Clin. Investig. *127*, 623–634. https://doi.org/10.1172/JCI88428.

43. Münz, M., Kieu, C., Mack, B., Schmitt, B., Zeidler, R., and Gires, O. (2004). The carcinoma-associated antigen EpCAM upregulates c-myc and induces cell proliferation. Oncogene *23*, 5748–5758. https://doi.org/10.1038/sj.onc.1207610.

44. Thuma, F., and Zöller, M. (2013). EpCAM-associated claudin-7 supports lymphatic spread and drug resistance in rat pancreatic cancer. Int. J. Cancer *133*, 855–866. https://doi.org/10.1002/ijc.28085.

45. Kuhn, S., Koch, M., Nübel, T., Ladwein, M., Antolovic, D., Klingbeil, P., Hildebrand, D., Moldenhauer, G., Langbein, L., Franke, W.W., et al. (2007). A complex of EpCAM, claudin-7, CD44 variant isoforms, and tetraspanins promotes colorectal cancer progression. Mol. Cancer Res. *5*, 553–567. https://doi.org/10.1158/1541-7786.MCR-06-0384.

46. Würfel, J., Rösel, M., Seiter, S., Claas, C., Herlevsen, M., Weth, R., and Zöller, M. (1999). Metastasis-association of the rat ortholog of the human epithelial glycoprotein antigen EGP314. Oncogene *18*, 2323–2334. https://doi.org/10.1038/sj.onc.1202542.

47. Stein, R., Chen, S., Sharkey, R.M., and Goldenberg, D.M. (1990). Murine monoclonal antibodies raised against human non-small cell carcinoma of the lung: specificity and tumor targeting. Cancer Res. *50*, 1330–1336.

48. Thomas, K.R., and Capecchi, M.R. (1987). Site-directed mutagenesis by gene targeting in mouse embryo-derived stem cells. Cell *51*, 503–512. https://doi.org/10.1016/0092-8674(87)90646-5.

49. Guerra, E., Lattanzio, R., La Sorda, R., Dini, F., Tiboni, G.M., Piantelli, M., and Alberti, S. (2012). mTrop1/Epcam knockout mice develop congenital tufting enteropathy through dysregulation of intestinal E-cadherin/beta-catenin. PLoS One *7*, e49302. https://doi.org/10.1371/journal.pone.0049302.

50. Trerotola, M., Guerra, E., Ali, Z., Aloisi, A.L., Ceci, M., Simeone, P., Acciarito, A., Zanna, P., Vacca, G., D'Amore, A., et al. (2021). Trop-2 cleavage by ADAM10 is an activator switch for cancer growth and metastasis. Neoplasia *23*, 415–428. https://doi.org/10.1016/j.neo.2021.03.006.

51. Carsana, L., Sonzogni, A., Nasr, A., Rossi, R.S., Pellegrinelli, A., Zerbi, P., Rech, R., Colombo, R., Antinori, S., Corbellino, M., et al. (2020). Pulmonary post-mortem findings in a series of COVID-19 cases from northern Italy: a two-centre descriptive study. Lancet Infect. Dis. *20*, 1135–1140. https://doi.org/10.1016/S1473-3099(20)30434-5.

52. Ambrogi, F., Fornili, M., Alberti, S., Querzoli, P., Piantelli, M., Pedriali, M., Boracchi, P., Biganzoli, E., and Coradini, D. (2013). EpCAM Expression is an Indicator of Increased Incidence of Relapse in p53-Positive Breast Cancer. Cancer Clin. Oncol. *2*, 41–50.

53. Tandon, A.K., Clark, G.M., Chamness, G.C., and McGuire, W.L. (1990). Association of the 323/A3 surface glycoprotein with tumor characteristics and behavior in human breast cancer. Cancer Res. *50*, 3317–3321.

54. Spizzo, G., Obrist, P., Ensinger, C., Theurl, I., Dünser, M., Ramoni, A., Gunsilius, E., Eibl, G., Mikuz, G., and Gastl, G. (2002). Prognostic significance of Ep-CAM AND Her-2/neu overexpression in invasive breast cancer. Int. J. Cancer *98*, 883–888. https://doi.org/10.1002/ijc.10270.

55. Jiang, L., Zhang, C., Li, Y., Yu, X., Zheng, J., Zou, P., Li, Y., Bin, X., Lu, J., and Zhou, Y. (2011). A non-synonymous polymorphism Thr115Met in the EpCAM gene is associated with an increased risk of breast cancer in Chinese population. Breast Cancer Res. Treat. *126*, 487–495. https://doi.org/10.1007/s10549-010-1094-6.

56. Relli, V., Trerotola, M., Guerra, E., and Alberti, S. (2019). Abandoning the Notion of Non-Small Cell Lung Cancer. Trends Mol. Med. *25*, 585–594. https://doi.org/10.1016/j.molmed.2019.04.012.

57. Piyathilake, C.J., Frost, A.R., Weiss, H., Manne, U., Heimburger, D.C., and Grizzle, W.E. (2000). The expression of Ep-CAM (17-1A) in squamous cell cancers of the lung. Hum. Pathol. *31*, 482–487. https://doi.org/10.1053/hp.2000.6711.

58. Girardet, C., Vacca, A., Schmidt-Kessen, A., Schreyer, M., Carrel, S., and Mach, J.P. (1986). Immunochemical characterization of two antigens recognized by new monoclonal antibodies against human colon carcinoma. J. Immunol. *136*, 1497–1503.

59. Pavšič, M., Gunčar, G., Djinović-Carugo, K., and Lenarčič, B. (2014). Crystal structure and its bearing towards an understanding of key biological functions of EpCAM. Nat. Commun. *5*, 4764. https://doi.org/10.1038/ncomms5764.

60. Gaber, A., Lenarčič, B., and Pavšič, M. (2020). Current View on EpCAM Structural Biology. Cells *9*, 1361. https://doi.org/10.3390/cells9061361.

61. Pathak, S.J., Mueller, J.L., Okamoto, K., Das, B., Hertecant, J., Greenhalgh, L., Cole, T., Pinsk, V., Yerushalmi, B., Gurkan, O.E., et al. (2019). EPCAM mutation update: Variants associated with congenital tufting enteropathy and Lynch syndrome. Hum. Mutat. *40*, 142–161. https://doi.org/10.1002/humu.23688.

62. Breast Cancer Association Consortium; Dorling, L., Carvalho, S., Allen, J., González-Neira, A., Luccarini, C., Wahlström, C., Pooley, K.A., Parsons, M.T., Fortuno, C., et al. (2021). Breast Cancer Risk Genes - Association Analysis in More than 113,000 Women. N. Engl. J. Med. *384*, 428–439. https://doi.org/10.1056/NEJMoa1913948.

63. Ng, P.C., and Henikoff, S. (2001). Predicting deleterious amino acid substitutions. Genome Res. *11*, 863–874. https://doi.org/10.1101/gr.176601.

64. González, B., Denzel, S., Mack, B., Conrad, M., and Gires, O. (2009). EpCAM is involved in maintenance of the murine embryonic stem cell phenotype. Stem Cell. *27*, 1782–1791. https://doi.org/10.1002/stem.97.

65. Guerra, E., Relli, V., Ceci, M., Tripaldi, R., Simeone, P., Aloisi, A.L., Pantalone, L., La Sorda, R., Lattanzio, R., Sacchetti, A., et al. (2022). Trop-2, Na(+)/K(+) ATPase, CD9, PKCalpha, cofilin assemble a membrane signaling super-complex that drives colorectal cancer growth and invasion. Oncogene *41*, 1795–1808. https://doi.org/10.1038/s41388-022-02220-1.

66. Alberti, S., Nutini, M., and Herzenberg, L.A. (1994). DNA methylation prevents the amplification of TROP1, a tumor-associated cell surface antigen gene. Proc. Natl. Acad. Sci. USA *91*, 5833–5837. https://doi.org/10.1073/pnas.91.13.5833.

67. Alberti, S., and Herzenberg, L.A. (1988). DNA methylation prevents transfection of genes for specific surface antigens. Proc. Natl. Acad. Sci. USA *85*, 8391–8394. https://doi.org/10.1073/pnas.85.22.8391.

68. Trerotola, M., Relli, V., Tripaldi, R., Simeone, P., Guerra, E., Sacchetti, A., Ceci, M., Pantalone, L., Ciufici, P., Moschella, A., et al. (2025). Large, recursive membrane platforms are associated to Trop-1, Trop-2, and protein kinase signaling for cell growth. Mol. Biol. Cell *36*, ar38. https://doi.org/10.1091/mbc.E24-06-0267.

69. Le Naour, F., and Zoller, M. (2008). The tumor antigen EpCAM: tetraspanins and the tight junction protein claudin-7, new partners, new functions. Front. Biosci. *13*, 5847–5865. https://doi.org/10.2741/3121.

70. Ovalle, S., Gutiérrez-López, M.D., Olmo, N., Turnay, J., Lizarbe, M.A., Majano, P., Molina-Jiménez, F., López-Cabrera, M., Yáñez-Mó, M., Sánchez-Madrid, F., and Cabañas, C. (2007). The tetraspanin CD9 inhibits the proliferation and tumorigenicity of human colon carcinoma cells. Int. J. Cancer *121*, 2140–2152. https://doi.org/10.1002/ijc.22902.

71. Ambrogi, F., Biganzoli, E., Querzoli, P., Ferretti, S., Boracchi, P., Alberti, S., Marubini, E., and Nenci, I. (2006). Molecular subtyping of breast cancer from traditional tumor marker profiles using parallel clustering methods. Clin. Cancer Res. *12*, 781–790. https://doi.org/10.1158/1078-0432.CCR-05-0763.

72. Guerra, E., Trerotola, M., Aloisi, A.L., Tripaldi, R., Vacca, G., La Sorda, R., Lattanzio, R., Piantelli, M., and Alberti, S. (2013). The Trop-2 signalling network in cancer growth. Oncogene *32*, 1594–1600. https://doi.org/10.1038/onc.2012.151.

73. Imbiakha, B., Sahler, J.M., Buchholz, D.W., Ezzatpour, S., Jager, M., Choi, A., Monreal, I.A., Byun, H., Adeleke, R.A., Leach, J., et al. (2024). Adaptive immune cells are necessary for SARS-CoV-2-induced pathology. Sci. Adv. *10*, eadg5461. https://doi.org/10.1126/sciadv.adg5461.

74. Van Delen, M., Janssens, I., Dams, A., Roosens, L., Ogunjimi, B., Berneman, Z.N., Derdelinckx, J., and Cools, N. (2022). Tolerogenic Dendritic Cells Induce Apoptosis-Independent T Cell Hyporesponsiveness of SARS-CoV-2-Specific T Cells in an Antigen-Specific Manner. Int. J. Mol. Sci. *23*, 15201. https://doi.org/10.3390/ijms232315201.

75. Fagiola, M., Reznik, S., Riaz, M., Qyang, Y., Lee, S., Avella, J., Turino, G., and Cantor, J. (2023). The relationship between elastin cross linking and alveolar wall rupture in human pulmonary emphysema. Am. J. Physiol. Lung Cell. Mol. Physiol. *324*, L747–L755. https://doi.org/10.1152/ajplung.00284.2022.

76. Fick, A. (1855). On liquid diffusion. London, Edinburgh Dublin Phil. Mag. J. Sci. *10*, 30–39. https://doi.org/10.1080/14786445508641925.

77. Pias, S.C. (2021). How does oxygen diffuse from capillaries to tissue mitochondria? Barriers and pathways. J. Physiol. *599*, 1769–1782. https://doi.org/10.1113/JP278815.

78. Al-Samir, S., Itel, F., Hegermann, J., Gros, G., Tsiavaliaris, G., and Endeward, V. (2021). O(2) permeability of lipid bilayers is low, but increases with membrane cholesterol. Cell. Mol. Life Sci. *78*, 7649–7662. https://doi.org/10.1007/s00018-021-03974-9.

79. Jones, D.L., Morley, M.P., Li, X., Ying, Y., Zhao, G., Schaefer, S.E., Rodriguez, L.R., Cardenas-Diaz, F.L., Li, S., Zhou, S., et al. (2024). An injury-induced mesenchymal-epithelial cell niche coordinates regenerative responses in the lung. Science *386*, eado5561. https://doi.org/10.1126/science.ado5561.

80. Gaiser, M.R., Lämmermann, T., Feng, X., Igyarto, B.Z., Kaplan, D.H., Tessarollo, L., Germain, R.N., and Udey, M.C. (2012). Cancer-associated epithelial cell adhesion molecule (EpCAM; CD326) enables epidermal Langerhans cell motility and migration in vivo. Proc. Natl. Acad. Sci. USA *109*, E889–E897. https://doi.org/10.1073/pnas.1117674109.

81. Winter, M.J., Nagelkerken, B., Mertens, A.E.E., Rees-Bakker, H.A.M., Briaire-de Bruijn, I.H., and Litvinov, S.V. (2003). Expression of Ep-CAM shifts the state of cadherin-mediated adhesions from strong to weak. Exp. Cell Res. *285*, 50–58. https://doi.org/10.1016/s0014-4827(02)00045-9.

82. Maetzel, D., Denzel, S., Mack, B., Canis, M., Went, P., Benk, M., Kieu, C., Papior, P., Baeuerle, P.A., Munz, M., and Gires, O. (2009). Nuclear signalling by tumour-associated antigen EpCAM. Nat. Cell Biol. *11*, 162–171. https://doi.org/10.1038/ncb1824.

83. Jiang, A., Bloom, O., Ono, S., Cui, W., Unternaehrer, J., Jiang, S., Whitney, J.A., Connolly, J., Banchereau, J., and Mellman, I. (2007). Disruption of E-cadherin-mediated adhesion induces a functionally distinct pathway of dendritic cell maturation. Immunity *27*, 610–624. https://doi.org/10.1016/j.immuni.2007.08.015.

84. Chen, H.N., Liang, K.H., Lai, J.K., Lan, C.H., Liao, M.Y., Hung, S.H., Chuang, Y.T., Chen, K.C., Tsuei, W.W.F., and Wu, H.C. (2020). EpCAM Signaling Promotes Tumor Progression and Protein Stability of PD-L1 through the EGFR Pathway. Cancer Res. *80*, 5035–5050. https://doi.org/10.1158/0008-5472.CAN-20-1264.

85. Guerra, E., Trerotola, M., Tripaldi, R., Aloisi, A.L., Simeone, P., Sacchetti, A., Relli, V., D'Amore, A., La Sorda, R., Lattanzio, R., et al. (2016). Trop-2 Induces Tumor Growth Through AKT and Determines Sensitivity to AKT Inhibitors. Clin. Cancer Res. *22*, 4197–4205. https://doi.org/10.1158/1078-0432.CCR-15-1701.

STAR★METHODS

KEY RESOURCES TABLE

REAGENT or RESOURCE	SOURCE	IDENTIFIER
Antibodies		
Anti-Trop-2	American Type Culture Collection (ATCC)	Cat# HB-187, RRID:AB_2287132
Anti-Trop-2	Guerra et al.[85]	T16; RRID:CVCL_N336
Anti-CD44	Santa Cruz Biotechnology	Cat# sc-52536, RRID:AB_629078
Anti-Trop-1/EpCAM (flow cytometry)	Klein et al.,[32]	HT-29/26; RRID:CVCL_J690
Anti-Trop-1/EpCAM (IHC)	Schon et al.,[41]	MH99; RRID:CVCL_C5W0
Anti-Trop-1/EpCAM (Western blotting)	Life technologies	Cat# MA5-29246, RRID:AB_2785146
Anti-CD9	Santa Cruz Biotechnology	Cat# sc-59140, RRID:AB_1120766
Anti-Ki67 (clone 30-9)	Roche	Cat# 05278384001, RRID:AB_2631262
Anti-E-cadherin (clone 36)	Roche	Cat# 05905290001, RRID:AB_3714871
Anti-β-catenin clone 14	Roche	Cat# 760–4242, RRID:AB_2861317
Biological samples		
Lung autoptic tissues	COVID-19 Siena Biobank	N/A
Chemicals, peptides, and recombinant proteins		
Crystal violet	Sigma	Cat# C-3886
Trypsin	Corning	Cat# 25–054-CI
Dulbecco's Modified Eagle Medium (DMEM)	Euroclone	Cat# ECM0060L
ES-grade fetal calf serum (FCS)	Gibco	Cat# 16141079
Leukemia inhibitory factor (LIF)	Merck	Cat# ESG1106
G418/geneticin	Life Technologies	Cat# 10131035
Ganciclovir	Life Technologies	Cat# 461710050
Lipofectamine 2000	Life Technologies	Cat# 11668030
Lipofectamine LTX	Life Technologies	Cat# 15338030
Critical commercial assays		
Alexa Fluor 488 carboxylic acid, succinimidyl ester	Life Technologies	A20000
Experimental models: Cell lines		
TBV-2 mouse embryonic stem cell (ES) cell line	Guerra et al.[49]	RRID:CVCL_0063
L cells (LTK-)	Alberti et al.[66]; Alberti and Herzenberg[67]	RRID:CVCL_3392
Mouse embryonic fibroblasts (MEF) – feeder layer	Guerra et al.,[49]	N/A
HEK-293T cells	Guerra et al.,[72]	RRID:CVCL_0063
KM12SM cells	Trerotola et al.[50]	RRID:CVCL_9548
Experimental models: Organisms/strains		
Mouse: 129S2/SvPas	Guerra et al.[49]	N/A
Oligonucleotides		
*TROP1/EPCAM*_Crispr1.for	5′ caccgGGCAAAAGTCGCCGTCGCCG 3′	N/A
*TROP1/EPCAM*_Crispr1.rev	5′ aaacCGGCGACGGCGACTTTTGCCc 3′	N/A
*TROP1/EPCAM*_Crispr2.for	5′ caccgGTGCACCAACTGAAGTACAC 3′	N/A
*TROP1/EPCAM*_Crispr2.rev	5′ aaacGTGTACTTCAGTTGGTGCACc 3′	N/A
Other		
gnomAD v2.1.1	Broad institute, ICGC	gnomad.broadinstitute.org/variant/2–47601106-T-C?dataset = gnomad_r2_1

(*Continued on next page*)

Continued

REAGENT or RESOURCE	SOURCE	IDENTIFIER
LOVD v.3.0 Build 30b	Global Variome Shared LOVD	databases.lovd.nl/shared/variants/EPCAM/unique
ClinVar GRCh38	ClinVar	www.ncbi.nlm.nih.gov/clinvar/
ICGC ARGO	International Cancer Genome Consortium Accelerating Research in Genomic Oncology (ICGC ARGO)	https://platform.icgc-argo.org
IntelliSite Image Management System	Philips	https://www.usa.philips.com/healthcare/product/FDP0912/intellisite-image-management-system
GEN-COVID Registry and Biobank	GEN-COVID consortium	https://sites.google.com/dbm.unisi.it/gen-covid
DNA sequences portal	cBioPortal for Cancer Genomics	www.cbioportal.org/datasets
Database of the Italian genetic variability	Network for Italian Genomes (NIG)	http://nig.cineca.it/
COVID-19 Host Genetics Initiative database	COVID-19 Host Genetics Initiative	https://www.COVID19hg.org/
Protein DataBank	RCSB PDB	https://www.rcsb.org/
NovaSeq6000 DNA sequencing System	Illumina	RRID:SCR_016387
Ventana BenchMark ULTRA IHC/ISH System	Roche	RRID:SCR_025506
FACS Canto II Cell Analyzer	BD Biosciences	N/A
FACS Aria III Cell Sorter	BD Biosciences	N/A
LSM-510 META confocal microscope	Zeiss	N/A
LSM-800 AiryScan confocal microscope	Zeiss	N/A
Pathology Scanner SG60	Philips	N/A
Recombinant DNA		
LentiCRISPRv2	Addgene	RRID:Addgene_52961
pVSVG	Addgene	RRID:Addgene_8454
psPAX2	Addgene	RRID:Addgene_12260
pΔEYFP/M-Mod	this paper	N/A
pΔEYFP/T-Mod	this paper	N/A
pFM54	Guerra et al.[49]	N/A
C57Bl/6J mouse bacterial artificial chromosome (BAC) clone RP24-315D17 GenBank AC163652.3))	BACPAC Resources Center (BPRC)	https://bacpacresources.org/
Software and algorithms		
PyMOL Version 2.0	Schrödinger, LLC.	http://www.pymol.org
Swiss PDB model	Expasy	https://swissmodel.expasy.org/
Fiji (ImageJ)	NIH	https://fiji.sc/
ZEN 2009 Light Edition	Zeiss	https://www.zeiss.com
VistaVision	ISS Inc.	https://www.iss.com
SimFCS 4	Lab. of Fluorescence Dynamics	https://www.lfd.uci.edu/
Sigma Stat 4.0	Systat Software, Inc.	https://systatsoftware.com
SIFT	SIFT	https://sift.bii.a-star.edu.sg/
SISA	SISA	https://www.quantitativeskills.com/sisa
QuPath	Open Software for Bioimage Analysis	https://qupath.github.io/
GraphPad Prism7	GraphPad Software, Inc.	https://www.graphpad.com
SPSS Version 15.0	SPSS, Chicago, IL	https://www.ibm.com/

EXPERIMENTAL MODEL AND STUDY PARTICIPANT DETAILS

Cell culture

L[66,67] and KM12SM[50] cells were grown in Dulbecco's Modified Eagle Medium (DMEM) supplemented with 10% (v/v) heat-inactivated fetal calf serum (FCS) at 37 °C in 5% CO_2. KM12SM and L cells were authenticated by short tandem repeat (STR) analysis (PowerPlex

16 System, Promega, and IDEXX Bioresearch, respectively), and further verified by morphology and flow cytometry assessment. Absence of mycoplasma contamination was routinely confirmed by PCR analyses and DAPI staining followed by fluorescence microscopy. L and KM12SM transfectants were seeded at 1.5-3.0 $\times 10^3$ cells/well in 96-well plates (five replica wells per data point). Cell growth was quantified at serial time points after seeding, by staining with crystal violet, upon normalization against standards of cell-reference curves of 2-fold serially diluted cell samples.

mTrop1 knockout cells

mTrop1 inactivation was obtained by targeted gene replacement in the TBV-2 mouse ES cell line from 129S2/SvPas mice, as described in Guerra et al.[49] The pFM54 vector was used for gene replacement. This vector contains positive (neomycin phosphotransferase cassette, *neo*) and negative (herpes virus thymidine kinase cassette, *TK*) selection, under mouse phosphoglycerokinase (*mPgk1*) promoters. ES cells were grown in DMEM supplemented with 15% (v/v) heat-inactivated ES-grade FCS and 1,000 units/ml leukemia inhibitory factor (LIF) (Esgro, Chemicon, Temecula, CA). Cells were cultured over a feeder layer of mitomycin-C-treated mouse embryonic fibroblasts (MEF). MEF were a kind gift by Lorenza Ronfani (Core Facility for Conditional Mutagenesis, IRCCS Ospedale San Raffaele, Milan, Italy). TBV-2 clones were selected in 200 μg/mL G418 (Invitrogen).

Samples and ethics clearance

Specimens were provided by the COVID-19 Biobank of Siena, which is part of the Genetic Biobank of Siena, member of BBMRI-IT, of Telethon Network of Genetic Biobanks (project no. GTB18001), of EuroBioBank. This study is part of the GEN-COVID Multicenter Study, https://sites.google.com/dbm.unisi.it/gen-covid, the Italian multicenter study aimed at identifying the COVID-19 host genetic bases. The GEN-COVID Multicenter Study was approved by the University Hospital (Azienda ospedaliero-universitaria Senese) Internal Review Board, n. 16917, March 16, 2020, Siena, Italy and by the local IRBs of all the recruiting hospitals involved.

METHOD DETAILS

Nomenclature

Trop-1 was originally identified in trophoblast cells.[66,67] The gene encoding Trop-1 is known by several alias, *TROP1/EPCAM/TACSTD1/M4S1/GA733-2* among others.[25] For the sake of clarity, in this article we only utilize the most frequently used ones, i.e., Trop-1[19,25]/EpCAM,[27] to refer to the protein, and *TROP1/EPCAM*, to refer to the gene.

Western blotting

Protein lysates were obtained from KM12SM cells by scraping them in lysis buffer containing 20 mM Tris-HCl (pH 7.4), 150 mM NaCl, 1 mM $CaCl_2$, 1 mM $MgCl_2$, 1% Triton X-100, and protease/phosphatase inhibitors. Lysates were separated by SDS-PAGE under non-reducing conditions using 12.5% acrylamide gels, then transferred onto nitrocellulose membranes. For Western blot analysis, membranes were incubated with primary antibodies for 3 h at RT, and with secondary antibodies for 1 h at RT.

Exome sequencing and statistical analysis

Whole exome sequencing with at least 97% coverage at 20x was performed, using the NovaSeq6000 System (Illumina, San Diego, CA, USA) as previously described.[8] A cohort of 2,446 SARS-CoV-2-positive subjects, collected within the GEN-COVID consortium was used to identify by machine learning algorithms the p.M115T Trop-1/EpCAM polymorphism as associated with worse disease outcome.[13–18] Details on polymorphisms/allele frequencies in the Italian population are presented in the Network for Italian Genomes (NIG; http://nigdb.cineca.it/) database.

Cancer genomic sequence data

Analysis for M115T (M/T) variant prevalence/function was conducted using the Repositories listed in the key resources table.

CRISPR-Cas9 inactivation of the *TROP1/EPCAM* gene expression

We ablated the expression of the endogenously expressed *TROP1/EPCAM* gene by CRISPR-Cas9, using two different sgRNAs targeting the *TROP1/EPCAM* gene. Knockout and transgenic cells were generated as follows:

L cells/transfectants - pΔEYFP empty vector.
L cells/*TROP1/EPCAM* transfectants - pΔEYFP/M-Mod.
L cells/*TROP1/EPCAM* transfectants - pΔEYFP/T-Mod.
KM12SM/*TROP1/EPCAM* Crispr1 #1.
KM12SM/*TROP1/EPCAM* Crispr1 #1/transgenic pΔEYFP/M-Mod.
KM12SM/*TROP1/EPCAM* Crispr1 #1/transgenic pΔEYFP empty vector.
KM12SM/*TROP1/EPCAM* Crispr2 #1.
KM12SM/*TROP1/EPCAM* Crispr2 #1/transgenic pΔEYFP/M-Mod pre-sorting.
KM12SM/*TROP1/EPCAM* Crispr2 #1/transgenic pΔEYFP/T-Mod pre-sorting.
KM12SM/*TROP1/EPCAM* Crispr2 #1/transgenic pΔEYFP empty vector.

Two CRISPR-Cas9 sgRNAs designed to target specific regions (exon 1 and exon 2) of the human *TROP1/EPCAM* gene were subcloned in the lentiviral vector LentiCRISPRv2, following the indicated procedure. The primer sequences introduced into the LentiCRISPRv2 vector are indicated in the key resources table. Packaging HEK-293 cells were co-transfected with the recombinant LentiCRISPRv2 and with the corresponding helper plasmids, pVSVG and psPAX2. Recombinant virions were collected from the tissue culture supernatants after 48 h, and used to infect the KM12SM target cells. After further 48 h, cells were selected using puromycin, and knockout stable cells were obtained. Cell populations bearing CRISPR-Cas9-inactivated *TROP1/EPCAM* genes were selected by flow cytometry, and confirmed devoid of surface Trop-1/EpCAM.

Expression vectors for the Thr115 (T-mod) as well as the Met115 (M-mod) variants of Trop-1/EpCAM were constructed to make these two variants mismatched and resistant to the CRISPR1 and CRISPR2 complexes targeting the endogenous *TROP1/EPCAM*. To this end three silent mutations were introduced in each CRISPR-targeted region of the T-mod and M-mod cDNAs (Figure S1).

Transfection of *TROP1/EPCAM* Met115 and Thr115 variants

Expression vectors for the T-mod as well as the M-mod variants of Trop-1/EpCAM were transfected in the murine fibrosarcoma L cells, which are devoid of endogenous expression of the *mTrop1/mEpcam* gene,[66,67] and in the KM12SM cells whereby the *TROP1/EPCAM* gene was inactivated by CRISPR-Cas9. Flow cytometry cell sorting of live transfectants using anti-Trop-1/EpCAM mAb selected transfected variants for parallel expression levels at the cell membrane.

COVID-19 patient lung histopathology and immunohistochemistry (IHC) analysis

Tissue specimens were fixed in 10% of neutral buffered formalin for 24–48 h. Hematoxylin and eosin stain was made from each lung tissue block. Histopathology parameters were compared across M/T heterozygous, M/M homozygous and T/T homozygous patients (Tables S1A and S1B).

IHC was carried out to quantify in lung tissue sections the expression of Trop-1/EpCAM (clone H99 at 1:1000 dilution for 30 min without antigen retrieval), E-cadherin (clone 36), β-catenin (clone 14), and the proliferative index by Ki67 labeling (clone 30-9). VENTANA detection kits and BenchMark IHC/ISH instruments were utilized. Microscope slide images were acquired with a Philips Pathology Scanner SG60. Images were managed and stored using the IntelliSite Image Management System (IMS). Images were obtained in.ndpi format and converted to.svg format for data presentation using QuPath. Object measurements were obtained with QuPath routines.

Comparative analysis of the Trop-1/EpCAM T115 and M115 structures

The crystal structure of the extracellular domain of Trop-1/EpCAM T115 (4MZV) was retrieved from the Protein DataBank. The 4mzv_T115 crystal structure was used as a template to obtain the model structure of the Trop-1/EpCAM M115, using the program Swiss pdb model. The Trop-1/EpCAM T115 and Trop-1/EpCAM M115 were overlaid with PyMol. Ramachandran plot analysis was conducted using Swiss pdb model.

Oxygen diffusion rates across cells

Oxygen diffusion across cells, cell layers and intercellular matrix obeys the fundamental laws of gas diffusion. According to Fick's first law,[76] when a convective term is negligible due to the high dilution of the gas in a cell, the gas flow J per unit surface area at steady state is:

$$J = \frac{C_2 - C_1}{l} D$$

Where l is the thickness of the cell, D is the mean diffusion coefficient, expressed in cm^2/s, C is the concentration of O_2 (C_2 in the lung alveoli, C_1 in the cell):

$$J = -D\left(\frac{\partial c}{\partial x}\right)_{T,p}$$

For constant absolute temperature T, and pressure p.

In the case of a pressure gradient Δp between external and internal membranes of the cell, the the gas flow per unit area is the permeability P multiplied by Δp, divided by the cell thickness l:

$$J = P\frac{\Delta p}{l}$$

The permeability of a gas can then be expressed as:

$$P = \frac{Jl}{\Delta p} = \frac{C_2 - C_1}{p_2 - p_1} D$$

As the solubility coefficient S of a gas at equilibrium is:

$$S = \frac{C}{p}$$

Permeability can be rewritten in the form:

$$P = DS$$

Hence, the O_2 permeability through a cell equals the mean O_2 diffusion coefficient multiplied by O_2 solubility.

The Fick's first law applies to stationary diffusion, whereby the concentration of the component that diffuses does not change over time. In the case of non-stationary systems, where the concentration varies in space and time, the Fick's second law applies, across area A, with flow J_{in} and J_{out}.

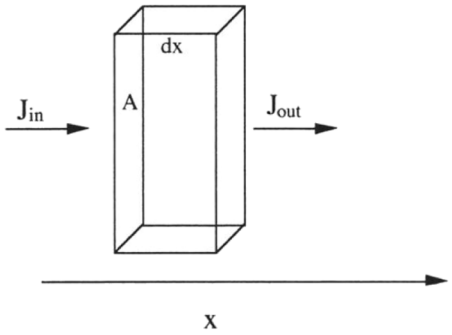

As:

$$dm = (J_{in} - J_{out})A\,dt$$

Hence:

$$\frac{\partial c}{\partial t} = -\frac{\partial J}{\partial x}$$

This is the so called equation of continuity. By substituting the expression of flow obtained from Fick's first law, the Fick's second law is:

$$\frac{\partial c}{\partial t} = D\frac{\partial^2 c}{\partial x^2}$$

Thus, the Fick's second law for oxygen diffusion across the thickness of alveolar membranes and of hyaline membranes is a second-order differential equation with respect to space and a first-order differential equation with respect to time.

The differential permeability of oxygen in lipids versus water limits the oxygen diffusion rates. According to the Meyer-Overton rule, the membrane permeability of a molecule is directly proportional to its lipid–water partition coefficient. Oxygen is ~25 times more soluble in lipids than in water, leading to oxygen diffusion in membranes at 26 cm/s for transbilayer and 36 cm/s for radial diffusion along the membrane midplane versus an overall diffusion rate 0.2 cm/s across alveolar membranes. Thus, limiting factors in oxygen diffusion are diffusion rates across water layers.[77,78]

QUANTIFICATION AND STATISTICAL ANALYSIS

The association of the p.M115T Trop-1/EpCAM polymorphism with disease outcome was confirmed by using the Chi-squared test.

IHC stainings for Trop-1/EpCAM, E-cadherin, and β-catenin for examined lung tissues were quantified on vascular endothelium, alveolar pneumocytes, ciliated epithelium, including intracellular localization. Staining intensity was classified as follows: absent: 0; focal ≤50% and diffuse: >50% of the cells. Trop-1/EpCAM IHC expression values were compared by Student's *t* test (Mean ± standard error of the mean (SEM)) and Mann-Whitney U Test.

SPSS was used throughout, and $p < 0.05$ was considered statistically significant. For Ki67, a dark brown diffuse or grainy nuclear staining was taken as positive. Ki67 labeling index (Ki67-LI) was assessed as described,[71] after identification of 'hot spots' using a 20× objective; Cells (including Ki67-positive cells) were counted in real time, and expressed as percentage. PI = [number of Ki67 positive cells ÷ number of cells scored]×100; 100 cells were scored in 3 different fields of view. All tissue section was separately evaluated by two pathologists (CB and NLF), who were unaware of the underlying clinicopathological characteristics of the patient.

Chemiluminescent signals from western blotting experiments were acquired using the Chemidoc Alliance Q9 digital platform. Band intensities were quantified using Fiji/ImageJ.